Clinical Implementation of a Real-Time Electromagnetic Localization System: Accuracy, Motion and Margin Analysis for IMRT and IMAT Treatments

by

Lauren D. Courlas

Medical Physics Graduate Program
Duke University

Date:_____

Approved:

_____
Jennifer O'Daniel, Ph.D., Supervisor

_____
Fang-Fang Yin, Ph.D., Chair

_____
Timothy Turkington, Ph.D.

Thesis submitted in partial fulfillment of
the requirements for the degree of Master of
Science in the Medical Physics Graduate Program
in the Graduate School of
Duke University

2010

ABSTRACT

Clinical Implementation of a Real-Time Electromagnetic Localization System: Accuracy, Motion and Margin Analysis for IMRT and IMAT Treatments

by

Lauren D. Courlas

Medical Physics Graduate Program
Duke University

Date:_____

Approved:

_____
Jennifer O'Daniel, Ph.D., Supervisor

_____
Fang-Fang Yin, Ph.D., Chair

_____
Timothy Turkington, Ph.D.

An abstract of a thesis submitted in partial
fulfillment of the requirements for the degree
of Master of Science in the
Medical Physics Graduate Program in the Graduate School
of Duke University

2010

Abstract

Accurate delivery of external beam radiation therapy relies on localization of the treatment target. Real-time electromagnetic localization systems (ELS) provide real-time tracking of the prostate during radiation therapy treatments using three implanted transponders. In this work, the Calypso® 4D Localization System™ (Calypso Medical, Seattle, WA), a commercial ELS, was evaluated. This study had four specific aims. First, the accuracy of the ELS for use in humans was verified through comparison with an on-board imaging kilo-voltage (kV) x-ray system used to produce both planar 2D orthogonal (planar) and volumetric 3D cone-beam computed tomography (CBCT) images. Second, the ELS was used to analyze prostate deformations and rotations occurring over the course of radiation therapy and the associated dosimetric impact was evaluated. Third, motion studies were conducted to investigate the use of the ELS during intensity-modulated arc therapy (IMAT) for prostate cancer. Fourth, appropriate planning margins were determined and new treatment plans utilizing a smaller planning margin were applied to weekly CBCTs for two patients who exhibited large transponder displacements (translational or rotational) to investigate the dosimetric effect of using smaller margins.

We found the electromagnetic alignments to be accurate to within 1 mm as compared to planar and CBCT image alignments. Changes in transponder geometry over the course of therapy seemed to be related to prostate volume reduction and

transponder implant location. All patients fell within the default geometric residual limit (2 mm) and most fell within the default rotational alignment limit (10°), though several patients exceeded the default rotational limit on multiple occasions and a CBCT image was acquired to verify the dosimetry when this occurred.

The majority of excursions occurring during an entire treatment session, when any repositioning was retrospectively removed, were less than 5 mm. The largest and most frequent excursions occurred in the anterior-posterior direction. The frequency of excursions was even smaller when considering only the first 120 seconds of a treatment session, to simulate an IMAT treatment. The majority of excursions occurring during the first 120 seconds of treatment were less than 4 mm. This indicates that the likelihood of having to interrupt the radiation delivery to reposition the patient during an IMAT treatment when a conventional 5 mm margin is used is very small.

Margin analysis using a formula developed by van Herk, et al., generated margins that were less than 3 mm for the majority of patients using actual motion data[1]. From the dosimetric analysis, a 3 mm margin appeared to be adequate when the main source of displacements was translational shifts. However, when large rotational displacements were observed, the 3 mm margin failed to maintain adequate prostate coverage. The treatment plan using a 5 mm margin, which was actually delivered during treatment, provided sufficient prostate coverage even in the presence of large rotational displacements. Multiple factors must be considered prior to implementing a

smaller planning margin and the margin may need to be determined on a patient-specific basis.

Contents

List of Tables

List of Figures

Acknowledgements

I would like to thank my advisor, Dr. Jennifer O'Daniel, for her guidance and unwavering support throughout this project. I would also like to thank Dr. Fang-Fang Yin for his advice and guidance. I am grateful to Dr. Robert Lee for contouring organ volumes on multiple CBCT scans for the dosimetric analysis. I would also like to thank Dr. Timothy Turkington for serving on my committee and providing useful suggestions to improve my project. Lastly, I would like to thank my family and friends for their support throughout this project.

1. Introduction

This section describes the prostate motion that occurs during a course of radiation therapy and discusses the dosimetric impact of this motion. An overview of the available methods of prostate alignment prior to radiation treatment is also presented. Next, a commercial real-time electromagnetic localization system (ELS), the Calypso® 4D Localization System™ (Calypso Medical, Seattle, WA), is introduced and past research involving this system is described. Treatment margins as well as the common treatment techniques are discussed to provide a rationale for the use of intensity-modulated radiation therapy (IMRT) and intensity-modulated arc therapy (IMAT) for the treatment of prostate cancer. Lastly, the specific aims and significance of this work are presented.

1.1 Background

1.1.1 Target Position Variation

Accurate delivery of external beam radiation therapy relies on accurate localization of the treatment target. The location of the treatment target may vary between treatment fractions (interfractional changes) as well as during a treatment fraction (intrafractional changes). Variation in prostate position over a course of radiation treatment for prostate cancer is caused by variations in bladder and rectal filling[2]. During an individual treatment fraction, prostate motion may be caused by rectal distention or other biological factors such as bladder volume changes[2,3,4].

Additionally, gradual pelvic muscle relaxation and leg motion can contribute to intrafraction motion[5,6]. Langen, et al., characterized two main types of prostate motions occurring during radiation therapy; these included a relatively slow drift away from the treatment isocenter or short sudden excursions that often resolved quickly with no intervention[5].

Both systematic and random errors account for the geometrical variations that occur during radiation therapy. Systematic errors tend to be consistent in magnitude and direction for a given patient and possibly for the patient population as a whole. Systematic errors can include target volume delineation from the planning computed tomography (CT) scan as well as a consistent shift (with respect to the isocenter) of the images obtained for daily alignment (caused by the imaging device). When the planning CT scan is acquired for treatment planning, the scan only displays the position of the prostate at a single time. Thus, delineation of the clinical target volume (CTV) from the planning CT scan accounts for a component of the systematic error because it is meant to represent the average prostate position. Additional systematic errors associated with the accuracy of aligning the patient to the CT scanner using lasers are also present. Random errors refer to day-to-day variations and they are not necessarily consistent in magnitude or direction[1]. Random variation includes daily setup errors as well as motion throughout radiation delivery. Discussion of treatment margins to account for the

systematic and random variations will be presented subsequently. The dosimetric impact of these variations is discussed in the next subsection.

1.1.2 Dosimetric Impact of Motion

Intrafractional and interfractional motion must be accounted for to ensure adequate coverage of the treatment target. If the target is not treated with the prescribed dose of radiation within reasonable limits, the cancer may not be fully eliminated and the probability of treatment failure may increase. Additionally, if motion causes the critical structure dose to increase, long term damage can result.

As mentioned previously, both systematic and random errors account for the geometrical variations during radiation therapy. The variations in treatment preparation cause a displacement of the dose distribution relative to the target volume. In contrast, treatment execution errors, including intrafractional and interfractional variation, cause a blurring of the dose distribution relative to the target volume [1,7]. van Herk, et al., determined that large random errors lead to a moderate underdosage for a large number of patients while large systematic errors lead to a significant underdosage for fewer patients[1].

When three-dimensional (3D) conformal and intensity-modulated radiation therapy techniques were introduced to provide better tumor control, studies were performed to assess the complications from delivering an increased dose to the patient. Acute and late bladder and rectal toxicity were the main concern when escalated doses

were delivered. Storey, et al., found that acute bladder toxicity and late rectal toxicity were correlated with the percentage of bladder or rectum treated to 70 Gy or more[8]. A common complication reported during dose escalation included late rectal bleeding that may have been related to the volume of rectum located within the high dose region as well as the overall dose[8]. Thus, reducing the amount of rectum and bladder exposed to high doses of radiation may reduce these complications. A study by Vargas, et al., produced similar results and found that the relative rectal wall and rectum volumes receiving doses of 50 – 72 Gy were strong predictors for chronic rectal toxicity[9]. These results can be applied similarly to the need to reduce or correct for prostate motion so that the rectum and bladder are not unnecessarily exposed to the highly conformal radiation field.

1.1.3 Prostate Alignment History

Several techniques have been utilized to align a patient prior to radiation therapy for prostate cancer. These techniques include the use of skin marks, planar images for bony alignment, ultrasound, CT and implanted fiducial markers[10]. Only the use of ultrasound, CT and implanted fiducials can account for the daily variation in prostate position (interfractional motion). Skin marks and portal images for bony alignment are not based on the position of the prostate itself, but rather on surrogate markers for the prostate (pelvic bones or skin). These surrogate markers are not necessarily indicative of

the position of the prostate because the prostate can move independently of this anatomy[11,12].

Ultrasound alignment is used to determine the shifts required to move the prostate into the same position as in the planning CT scan prior to each treatment session[10]. Using CT alignment, the prostate is contoured on the planning CT image and this contour is overlaid on the daily CT image. The prostate volume on the daily CT image is aligned with the contour and the patient is shifted accordingly. Wong, et al., determined the location of the CTV and rectum on daily CT images and by comparing these to the planned positions, determined a new isocenter for treatment[12]. This group aligned their patients using skin marks and then acquired daily CTs during five treatment sessions for each patient (total of 540 CT scans). They found that in the anterior-posterior (AP, vertical) direction, 54% of patients required a shift ≥ 3 mm, 44% required a shift > 5 mm and 15% required a shift > 10 mm after alignment with skin marks. In the superior-inferior (SI, longitudinal) direction, 27% of patients required a shift > 3 mm, 25% required a shift > 5 mm and 4% required a shift > 10 mm. In the right-left (RL, lateral) direction, 34% of patients required a shift > 3 mm, 24% required a shift > 5 mm and 5% required a shift > 10 mm[12].

Additionally, radiopaque markers implanted in the prostate have frequently been used for localization of the prostate[4]. The implanted radiopaque markers serve as a surrogate for the prostate. The position of the prostate is then determined prior to the

delivery of radiation using imaging techniques such as on-board kilo-voltage (kV) x-ray systems used to produce both planar 2D orthogonal (planar) or cone-beam CT (CBCT) images, as well as megavoltage (MV) planar or CT imaging systems. Litzenberg, et al., used this system of localization and determined that the positioning of a patient using only skin marks resulted in large errors (average of -5.41 mm AP) that could be reduced substantially with the use of radiographic localization of the implanted markers (average of -2.31 mm AP)[4]. The large residual displacements observed by Litzenberg, et al., and Wong, et al., after alignment with skin marks illustrate the importance of using a localization method that accounts for interfractional variation.

O'Daniel, et al., performed a dosimetric comparison of four alignment techniques for prostate cancer radiation therapy that included skin marks, bony alignment from portal images, CT and ultrasound[10]. This group found that CT alignment resulted in the most consistent results, however it is the most expensive technique to implement. The greatest dosimetric benefits were seen when CT alignment was used, followed by ultrasound, bone and skin alignments[10]. This group determined that prostate coverage was adequate for 70%, 90% and 100% of patients using skin and bone alignments, ultrasound alignment, and CT alignment, respectively[10].

Intrafractional prostate motion also occurs, but it is smaller in magnitude than the daily variations in prostate location, making it harder to observe than interfractional displacements[2]. This intrafractional motion must be accounted for during highly

conformal intensity-modulated radiation therapy treatments to ensure that the target receives the prescribed dose while the dose to critical structures is minimized. Critical structures in the treatment of prostate cancer include the rectum, bladder, femoral heads and penile bulb. If intrafractional motion is accounted for, treatment margins could be reduced, which may decrease the dose to the rectum and bladder and may allow for an increased dose to be delivered to the target. The ability to localize the target prior to radiation treatment using the methods discussed above also affects the size of treatment margins.

1.1.4 Electromagnetic Localization System

1.1.4.1 Clinical Benefit

An electromagnetic localization system (Calypso 4D Localization System) was developed as an alternative method to implanted radiopaque markers for localization of the target in the treatment of prostate cancer. In addition to localization, this system also allows real-time tracking of the target in three-dimensions using three implanted electromagnetic transponders. Several major benefits of the ELS as compared to traditional radiopaque markers exist. First, the ELS does not use ionizing radiation for localization, in contrast to x-ray based techniques[2]. Second, the system does not require an in depth image acquisition and registration process and thus may be faster and simpler for the radiation therapists to use for localization. Lastly, the ELS allows for real-time tracking of the target throughout the entire course of treatment rather than solely

allowing for localization of the target prior to treatment[2]. Several disadvantages of the ELS exist and these include the invasive nature of the transponder implant procedure and the severe image artifacts caused by the transponders in MR images, which prevents the use of MRI for post-treatment follow-up studies.

1.1.4.2 Past Research

Though past studies involving the motion of the prostate between treatment fractions had been performed, fewer data were available on the continuous motion of the prostate during a single treatment fraction prior to the introduction of the ELS. The first human study involving the ELS by Willoughby, et al., found that the majority of patients' prostates remained relatively stable during the tracking session. However, several patients did demonstrate significant motion[2]. Willoughby, et al., found that the average maximum difference in the calculated centroid of the transponders for all patients was 3.61 ± 3.13 mm and 3.92 ± 4.32 mm in the longitudinal and vertical directions, respectively, while it was only 0.91 ± 0.35 mm in the lateral direction[2].

More recently, Langen, et al., analyzed the motion of the prostate using ELS tracking data from 17 patients[5]. They found that on average, the prostate was displaced by > 3 mm and > 5 mm roughly 14% and 3% of the time, respectively. Their study also indicated that the probability of displacement of the prostate increased with time after the initial localization[5]. The intrafractional prostate motion quantified by these groups indicates the importance of continuous monitoring throughout treatment. Another

group indicated that pre- and post-treatment imaging is not an adequate method for predicting intrafractional prostate motion[13]. Noel, et al., also found that even intermittent imaging during a treatment session is only a true predictor of prostate motion if it is performed at a high enough rate, again supporting the need for continuous monitoring of the prostate position[13].

1.1.4.3 Clinical Use

To use the ELS for localization and tracking, three electromagnetic transponders must be implanted in or near the prostate at least one week prior to the simulation (planning) CT scan. The three transponders are generally implanted in the apex, left base and right base regions of the prostate, as indicated in Figure 1, below, and are radiopaque so they can be viewed on radiographic images.

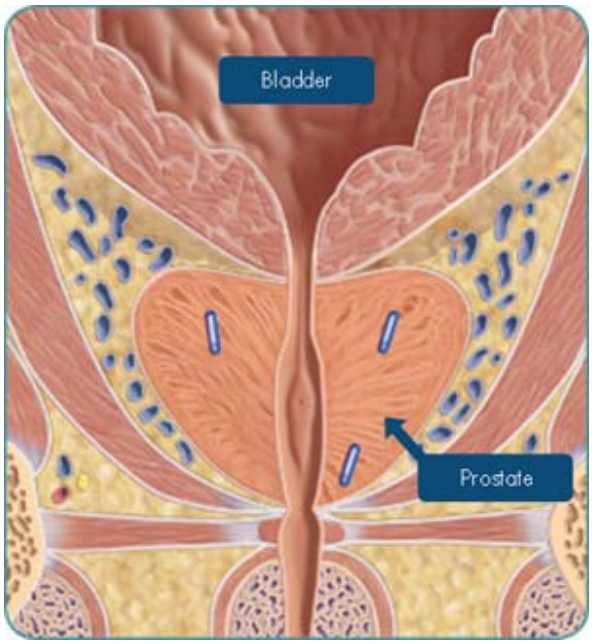

Figure 1: Coronal view of preferred transponder locations in the prostate. Image copied with permission from Calypso Medical[14].

The transponders are cylindrically shaped and are 8 – 8.7 mm in length and 1.85 mm in diameter, as displayed in Figure 2, below. The transponders are glass encapsulated and consist of a passive inductance-resistance-capacitance (LRC) circuit containing a ferromagnetic inductor[15]. The transponders do not contain an internal energy source and each transponder has a distinct resonant frequency[15,16]. The transponder coordinates relative to the target isocenter are determined during the treatment planning process from the planning CT scan[16].

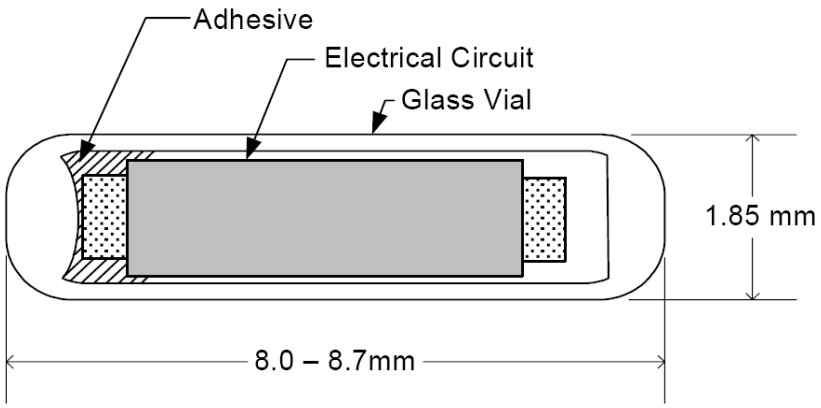

Figure 2: Electromagnetic Transponder. Image copied from Calypso User's Manual (ASM0078-004, Page 2-4) with permission from Calypso Medical[16].

To determine the position of the implanted transponders during a treatment session, an AC magnetic array is placed over the patient that creates non-ionizing electromagnetic fields at varying frequencies to excite the transponders[17,18]. This array contains four source and 32 receiver coils[17]. Nine optical targets are embedded within the array and communicate with the optical system composed of three infrared cameras to determine the array position relative to the machine isocenter[16]. A schematic of the Calypso 4D Localization System is displayed in Figure 3. This ELS is composed of the Electromagnetic Transponders, the 4D Electromagnetic Array, three infrared cameras, the 4D console located in the treatment room and the 4D tracking station located at the treatment console outside of the room.

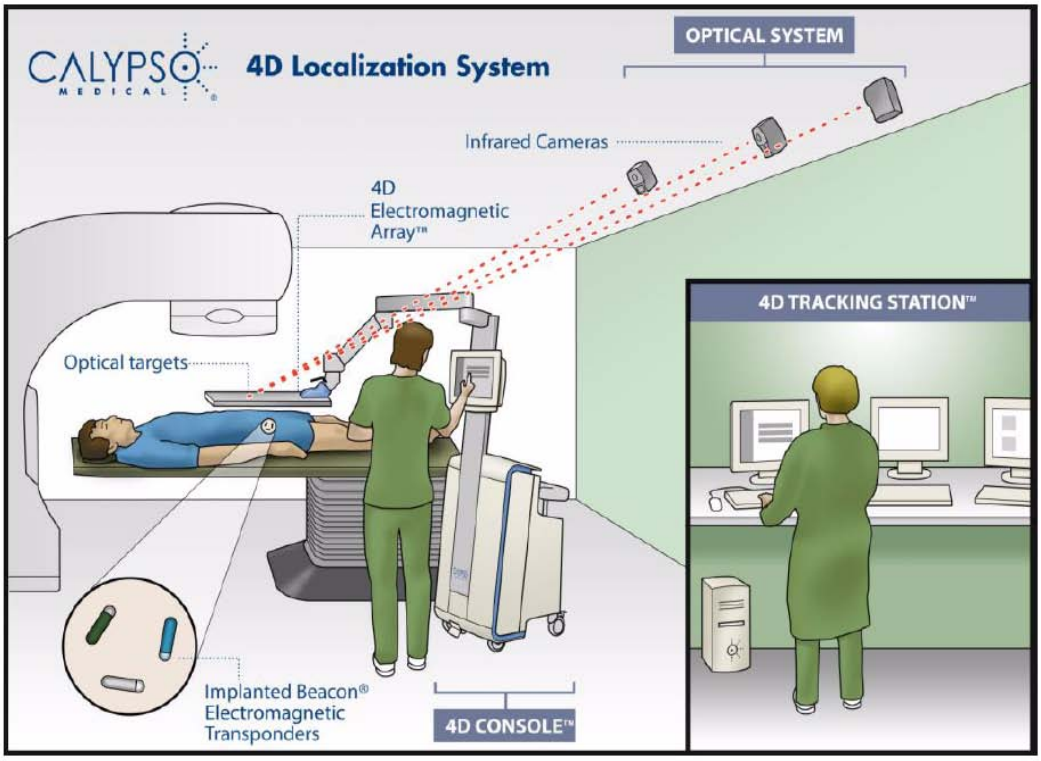

Figure 3: Calypso 4D Localization System Components. The main components of the system include Implanted Electromagnetic Transponders, 4D Electromagnetic Array, Infrared Cameras, 4D Console and the 4D Tracking Station. Image copied from Calypso User's Manual (ASM0078-004, Page 2-3) with permission from Calypso Medical[16].

The source coils within the 4D Electromagnetic Array generate an oscillating electromagnetic field at three unique frequencies in the range of 275 – 550 kHz to cyclically excite the transponders by inducing resonance. Once the electromagnetic field is turned off, the excited transponders release their stored energy through creating oscillating electromagnetic fields. The transponder signals during relaxation are detected by the receiver coils within the array and are used to determine the position and orientation of each transponder with respect to the array[16,17].

Using the transponder signals detected by the array, the offset of the treatment isocenter from the mechanical isocenter is determined and reported at a rate of 10 Hz[17]. Prior to radiation delivery, this offset is used to align the target to the mechanical isocenter. If the allowed offset of the target is exceeded during treatment, the radiation therapists realign the patient.

1.1.4.4 Initial Accuracy Validation

The accuracy of the ELS was first evaluated by Balter, et al., who demonstrated the submillimeter accuracy of the system by comparing known and measured locations of the transponders within phantoms[17]. The accuracy of the tracking feature of the ELS was also verified using a dynamic phantom which moved in a circular path[17]. It should be noted that Balter, et al., placed the transponders in a 0.9% saline solution for their study to simulate a conductivity environment that was twice that of human tissue. Balter, et al., determined the precision of the ELS position readout at varying distances from the array by placing a transponder at 80 mm and 270 mm from the array and monitoring the position with the ELS for periods up to 20 minutes. These distances represent the expected range of transponder locations relative to the array based on CT image analysis for previous prostate cancer patients. Balter, et al., found the precision of the ELS position measurements to be 0.006 mm, 0.01 mm and 0.006 mm about the x, y and z axis, respectively, for the transponder located 80 mm from the array. For the transponder located 270 mm from the array, the precision of the measurements was

slightly larger and was 0.27 mm, 0.36 mm and 0.48 mm about the x, y and z axis. The z axis was defined perpendicular to the array, while the x-y plane was defined as the plane parallel to the array[17]. These values indicate that the precision of the ELS measurements increases slightly with the distance of the transponder from the array.

The accuracy of the system in humans was evaluated by comparing 44 electromagnetic alignments with the corresponding kV x-ray alignment for 11 patients in a study by Willoughby, et al. The average difference between the two alignment methods was 1.5 $\pm$ 0.9 mm and the time between the electromagnetic and planar x-ray alignments was roughly 3 to 5 minutes[2].

A larger multi-institutional study was later performed which compared the electromagnetic alignments with alignments determined by a kV x-ray based system for 35 patients[3]. The comparisons were made four times during six fractions for each patient. The ELS and x-ray measurements corresponded to slightly different time points because the ELS measurements were obtained from inside the treatment room while the x-ray based alignments were obtained from outside the treatment room. The two measurements were separated by 2.53 minutes on average. Over 1000 comparisons between the ELS and x-ray system were made and it was found that the average differences between the alignments were -0.1 $\pm$ 0.9 mm, -0.4 $\pm$ 1.4 mm and 0.0 $\pm$ 1.3 mm in the lateral, longitudinal and vertical directions, respectively[3]. Additionally, Kupelian, et al., evaluated the stability of the transponders within the prostate and found that the

mean standard deviation of the intertransponder distances from 4 days post implant to the last treatment fraction was only 0.8 mm[3]. This indicated to us that implanted transponders are stable over the course of radiation therapy.

Santanam, et al., also performed a study to evaluate the accuracy of the ELS by comparing the measured displacements to known transponder positions within a phantom[18]. This group found the root mean square difference between the electromagnetic alignments and the known trajectory of a four-dimensional phantom to be 0.33 mm. In a static phantom they calculated a root mean square difference less than 0.1 mm[18].

1.1.5 Margins in Radiation Therapy

Geometrical uncertainties in radiation therapy include target volume delineation, organ motion and setup accuracy[1]. Setup inaccuracies can include intrafractional motion or deformations, the error of the imaging device used for localization and the error associated with applying any corrective repositioning[19]. Margins are used to ensure that the correct dose is delivered to the target in the presence of various geometrical uncertainties.

Several volume definitions and associated margin definitions are used in radiation therapy planning. These volumes include the gross tumor volume (GTV), clinical target volume and planning target volume (PTV) and are defined by the International Commission on Radiation Units and Measurements (ICRU) Report 50 and

are determined individually for each patient by the radiation oncologist. The GTV refers to the volume containing known tumor. The CTV expands upon the GTV and contains the volume of suspected microscopic spread[20]. The CTV must receive an adequate radiation dose for the disease to be cured. Lastly, the PTV expands upon the CTV to account for geometrical uncertainties and inaccuracies to ensure that the CTV receives the prescription dose[1,20]. The Duke University Department of Radiation Oncology utilizes a 5 mm isotropic CTV-to-PTV planning margin (referred to hereafter as "planning margin") for prostate cancer patients for whom the ELS is being used. This margin was determined to be adequate for our institution after consulting with genitourinary radiation oncologists and radiation therapy physicists.

Studies have been performed to develop margin formulations for use in radiation therapy. A commonly used margin equation developed by van Herk, et al., utilizes the probability of target volume coverage to determine appropriate planning margins numerically[1]. This group used a threshold in their margin formulation that required the minimum dose to the CTV to be 95% of the prescription dose or higher for 90% of the population[1]. In the margin equation determined by van Herk, et al., the systematic and random variations, as described previously, are separated. Typically, the margin necessary to account for systematic errors is much larger than that for random variations in prostate location[1]. It should be noted that the margin equation used in this study does not account for rotational errors or shape variations of the prostate[1].

1.1.6 Treatment Techniques

Several modern treatment techniques are currently used in radiation therapy. These include three-dimensional conformal radiation therapy, intensity-modulated radiation therapy and intensity-modulated arc therapy. 3D conformal radiation therapy utilizes 3D anatomic information from CT images to conform the radiation dose to the target volume while delivering the minimum dose to normal structures. Target volumes and relevant critical structures are contoured on the planning CT by the radiation oncologist. Each treatment field is shaped to include the PTV (as seen from the beam's-eye-view of that field) with a margin that will allow a sufficiently high dose distribution to cover the PTV when penumbra effects are considered[21].

IMRT uses similar concepts as 3D conformal radiation therapy, however, the intensity within each treatment field is modulated to produce an optimized dose distribution within the target. This method of treatment utilizes "inverse planning" techniques, in which the treatment planner specifies various factors (number of treatment fields, beam angles, target minimum/maximum dose constraints, critical structure dose constraints, etc.) and the treatment planning system creates optimized fluence profiles. IMRT provides more conformal dose distributions than 3D conformal radiation therapy, and is thus more susceptible to the dosimetric effects of interfractional and intrafractional target position variations[21].

IMAT (e.g., Varian RapidArc) is a newly developed treatment technique that delivers a conformal dose distribution to the target during a continuous 360-degree rotation of the linear accelerator gantry, allowing for a significantly shorter treatment time as compared to IMRT. The gantry rotation speed, MLC shape and dose rate can be varied during the treatment plan optimization. Given the significantly shorter IMAT delivery time, the dosimetric impact of an intrafractional excursion would be greater for IMAT than for conventional IMRT. While it is possible to interrupt the delivery and reposition the patient during an IMAT treatment, the procedure is time-consuming and is best to avoid if possible. To resume the radiation delivery after an interruption, the gantry must be reset to its initial position and must rotate through the already delivered treatment beam angles prior to beginning delivery. Hence, appropriate margins should be chosen such that the probability of a significant excursion during treatment is minimal.

IMRT is most commonly used to treat prostate cancer patients, with IMAT becoming a more popular option because of its efficiency. Both IMRT and IMAT treatments are used in the Duke University Department of Radiation Oncology for the treatment of prostate cancer.

1.2 Specific Aims

There were four main goals of this work. First, the accuracy of a commercial ELS for human use was verified by comparing it with an on-board kV x-ray system used to produce both planar 2D orthogonal and volumetric 3D CBCT images.

Second, the interfractional displacement of the transponders implanted in the prostate, including both positional and rotational reproducibility relative to their initial location, was analyzed. The patient-specific causes of variations in these measurements were also investigated. Observed anatomical deformations occurring over the course of radiation therapy were analyzed to determine the associated dosimetric impact.

Third, motion studies were conducted to investigate the use of the ELS for continuous localization during IMAT treatments of prostate cancer. The goal of these studies was to quantify the amount of motion that occurred during the first 120 seconds of the original ten patients' treatments (simulating an IMAT delivery), and determine the minimum appropriate margin to account for intrafractional motion such that the majority of the excursions would not have a detrimental dosimetric impact.

Fourth, appropriate treatment planning margins were determined for each of the ten patients and for the population as a whole using a margin formula developed by van Herk, et al[1]. New treatment plans utilizing a 3 mm planning margin were then created and applied to the weekly CBCT scans for two patients who exhibited large rotations or prostate deformations. The goal of this part of the study was to determine if smaller

margins would result in a decreased dose to the rectum and bladder while maintaining coverage of the prostate. Additionally, the effect of large rotations or prostate deformations in the presence of a smaller margin was evaluated. The treatment plan actually delivered to the patients used a 5 mm planning margin.

1.3 Significance

Verifying the accuracy of the ELS using CBCT imaging was unique to this work and provided similar results to our analysis involving planar imaging as well as to previous studies. The ELS provides an alternative option to localization with planar or CBCT images and delivers no additional dose to the patient. It also uniquely provides continuous tracking of the prostate throughout treatment which could allow for smaller planning margins since any substantial excursion from the planned treatment position would be accounted for by realigning the patient prior to delivering the next radiation field. After verifying the accuracy of the ELS, this localization and tracking system was fully implemented in the Duke University Department of Radiation Oncology as a viable alternative to gold seed implantation and localization through planar or CBCT images for prostate cancer patients.

In addition to using the CBCT scans to verify the accuracy of the ELS, these scans were also used to investigate prostate deformations and rotations. By analyzing the deformations and rotations occurring over the course of radiation therapy using both the CBCT and ELS data, we hoped to determine the patient-specific causes of these

variations. Then, investigating the dosimetric consequences of these variations, if any, would provide insight into whether adequate coverage of the target was still attained and whether the dose to critical structures had increased as compared to the original treatment plan. Another component to the dosimetric analysis included simulating treatment plans using smaller planning margins. Smaller margins could provide a dosimetric benefit to the rectum and bladder, however, adequate coverage of the target must still be maintained. Smaller margins may also allow for hypofractionation, in which a higher dose is delivered to the target in fewer fractions than in conventional radiation therapy. Hypofractionation is more convenient for the patient but this method of treatment is only possible if the dose to normal structures is minimized to limit the toxicity that may be caused by a higher dose per fraction. Smaller margins are more feasible using the ELS for continuous tracking throughout treatment because intrafractional motion can be corrected for.

Lastly, the motion studies performed in this work provided results which indicated that the ELS could be used for localization and tracking during IMAT treatments because the probability of a significant target excursion during an IMAT delivery was extremely small. This is clinically beneficial because IMAT treatments are a more convenient and efficient alternative to standard IMRT treatments because of a significantly shorter treatment time.

2. Materials and Methods

Sixteen prostate cancer patients were implanted with three electromagnetic transponders in the apex, right base, and left base sections of the prostate one week prior to simulation (planning) CT scans for radiation therapy. In one patient (Patient 1), one transponder was lost prior to the simulation CT scan, so that only two were usable. Localization and continuous tracking using the ELS were performed for all 16 patients.

All radiation therapy plans were designed in the Eclipse v8.6 treatment planning system (Varian Medical Systems Inc., Palo Alto, CA). Intensity-modulated radiation therapy was used to maximize the tumor dose coverage while minimizing the dose to the bladder, rectum, and femoral heads. The PTV for the primary plan covered the prostate and seminal vesicles plus a 5 mm isotropic margin. The majority of patients received 54 Gy in 27 fractions to the PTV. A boost plan was then delivered to a new PTV that encompassed the prostate plus a 5 mm isotropic margin and delivered 22 – 24 Gy in 11 – 12 fractions for the majority of patients. The total dose delivered to the prostate was 76 – 78 Gy for these patients.

2.1 Electromagnetic Localization System Accuracy Verification

In order to verify the accuracy of the ELS, displacements based on the tracking report from the ELS were compared to displacements based on planar images and to displacements based on CBCT imaging. The ELS was used for the initial localization and the first group of ten patients received daily planar orthogonal (AP and right lateral)

images to confirm the localization of the target. The planar images were taken before and after each radiation treatment while electromagnetic tracking data were collected. The remaining six patients received weekly pre-treatment CBCT scans while electromagnetic tracking data were collected.

The displacements as measured by the planar images and CBCT scans were compared to those measured by the ELS. Over 550 planar orthogonal image pairs (from Patients 1 – 10, excluding Patent 6) and 25 CBCT images (from Patients 11 – 16) were analyzed using Offline Review software (Varian Medical Systems, Inc., Palo Alto, CA) to determine the displacement of the prostate at the time each image was acquired. The imaging data for Patient 6 could not be analyzed because the transponder contours from the planning CT were not visible in Offline Review.

Offline Review provides the time corresponding to when the image was acquired in relation to the time of the first and last radiation beam-on. Using this information, the target displacement in the lateral and vertical directions measured by the ELS within +/- 1 second of the planar image acquisition was determined. The displacement in the longitudinal direction measured by the ELS within +/- 15 seconds of the planar images was also determined. The displacement in the lateral direction was determined from the AP image, while the displacement in the vertical direction was determined from the lateral image. The displacement in the longitudinal direction was determined using both the AP and lateral planar images. Thus, the average of the acquisition times for the

lateral and AP images (acquired roughly 30 seconds apart) was used to determine the corresponding ELS measured displacement in the longitudinal direction.

A difference exists between the actual time a CBCT image is acquired and the acquisition time reported in Offline Review. This time difference was determined by performing a phantom study and then the correct time of the CBCT scan acquisition was used to determine the corresponding ELS measured displacement.

An image of the Offline Review user interface is displayed in Figure 4, below. The radiopaque transponders on the daily planar images were manually aligned to the transponder contours from the digitally reconstructed radiographs (DRRs) created from the planning CT scan and the displacements in the vertical, longitudinal and lateral directions were calculated and displayed by Offline Review. The radiopaque transponders on the weekly CBCT images were manually aligned to the transponders in the planning CT and the displacements in the vertical, longitudinal and lateral directions were calculated and displayed by Offline Review.

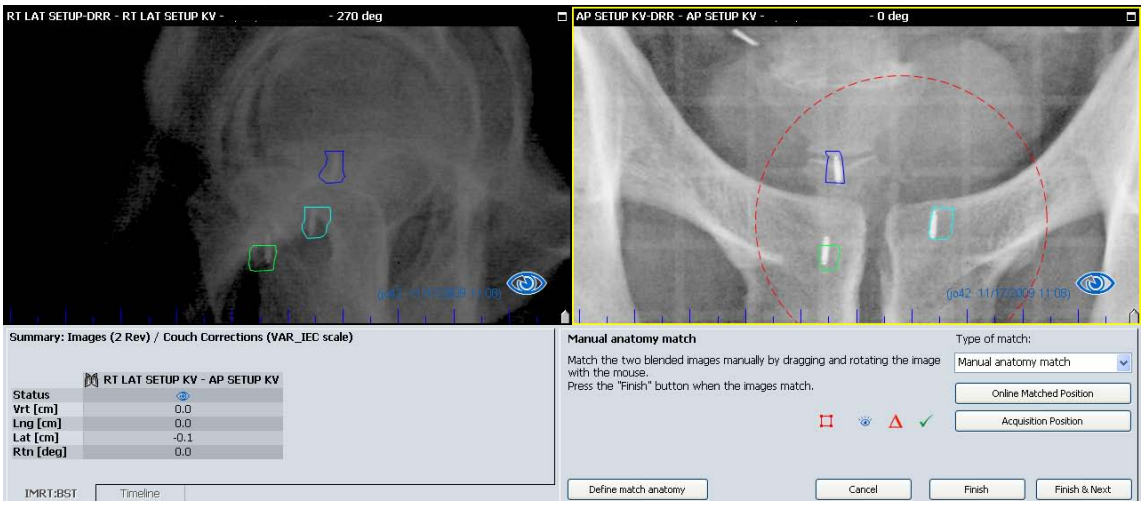

Figure 4: Offline Review User Interface. The contours of the three transponders are displayed in color and overlaid on the planar orthogonal images.

The tracking data from an ELS session report are presented in Figure 5, below. This figure displays the lateral, longitudinal and vertical tracking data for the duration of the treatment session. The periods of radiation delivery are displayed as gray bars on each plot. The raw tracking data were converted into Microsoft Excel format, and provided submillimeter positioning information with a time resolution of 0.1 seconds. The ELS measured displacement at the time corresponding to the planar or CBCT image acquisition was recorded and used in the comparison.

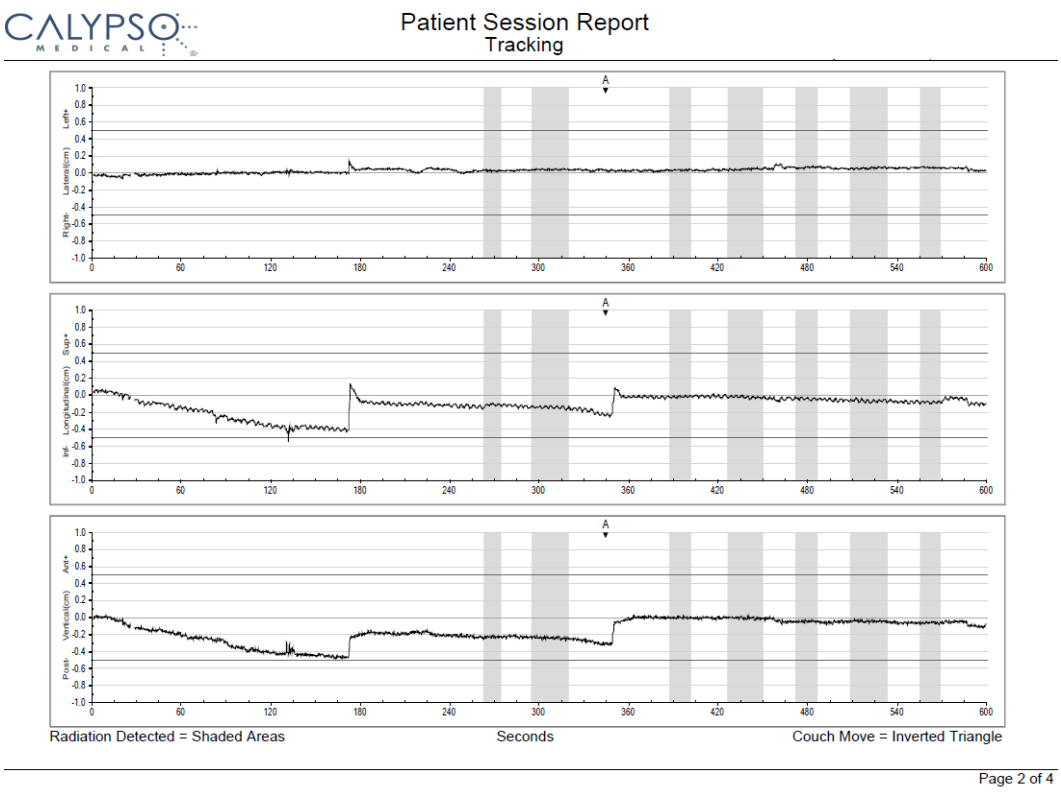

Figure 5: Tracking data from Calypso system session report.

The student's paired two-tailed t-test was used for statistical analysis of the ELS and x-ray system measured displacements. The t-test analyzes two sets of values to determine if the population means are equal. The test gives the probability that the observed difference in the two population means is insignificant (i.e. due to chance alone). The paired t-test is used when the two sets of values are related in some way. In this work, the two sets of values corresponded to target displacements for the same patient and time as measured by two different methods (ELS and x-ray system), and thus the values were correlated. The hypothesized mean difference at which the ELS and planar or CBCT measured displacements were indistinguishable ($p > 0.05$) was

determined for the population. The hypothesized mean difference at which the ELS and planar image measured displacements were indistinguishable was also found for each patient (Patients 1 – 10, excluding Patient 6) individually.

2.2 Positional and Rotational Reproducibility of Transponders

The ELS generates session reports for each patient after every treatment session and a portion of one of these reports is displayed below in Figure 6. The session reports include the planned and measured intertransponder distances, the rotational alignment of the prostate, the geometric residual and continuous tracking data. They also include the magnitude of the adaptive couch shifts, if any repositioning was performed.

Localization Summary

Isocenter Localization	Lat(Left+)	Long(Sup+)	Vert(Ant+)
Shift from Initial Setup (cm):	-0.39	0.93	0.80
Confirmed Isocenter Offset (cm):	-0.04	0.00	-0.01
Time:			

Intertransponder Distances	Planned	Measured
Apex to Left Base (cm):	2.61	2.42
Right Base to Left Base (cm):	2.44	2.26
Apex to Right Base (cm):	2.30	2.10

	Limit	Measured
Geometric Residual (cm):	0.20	0.11
Rotation - Pitch (deg):	10.0	-3.0
Rotation - Roll (deg):	10.0	0.7
Rotation - Yaw (deg):	10.0	-2.2

Figure 6: Portion of Calypso system session report including intertransponder distances, geometric residual and rotational alignment.

The geometric residual refers to the root mean squared difference between the daily and reference transponder positions after performing a best-fit alignment[16]. Figure

7, below, displays an example of the variation that could occur between the reference and daily transponder positions.

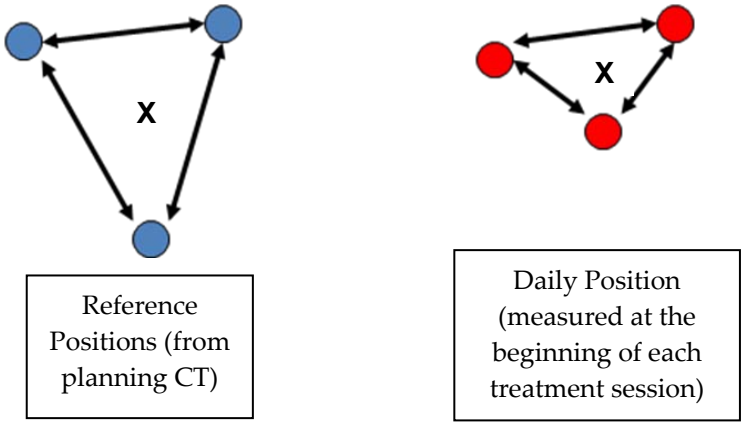

Figure 7: Example of variation that can occur between reference and daily transponder positions. The ELS uses this difference between the reference and daily transponder positions, after performing a best-fit alignment, to calculate the geometric residual.

Rotation refers to the rotation of the three-transponder system about isocenter, relative to its reference position. For patients with three implanted transponders (Patients 2 – 10), the rotational alignment is given in three directions (pitch, roll and yaw). Rotational information in all three directions could not be calculated if only two transponders were present (Patient 1). A diagram displaying the target rotations that result in a positive rotation measurement by the ELS is given below in Figure 8[22].

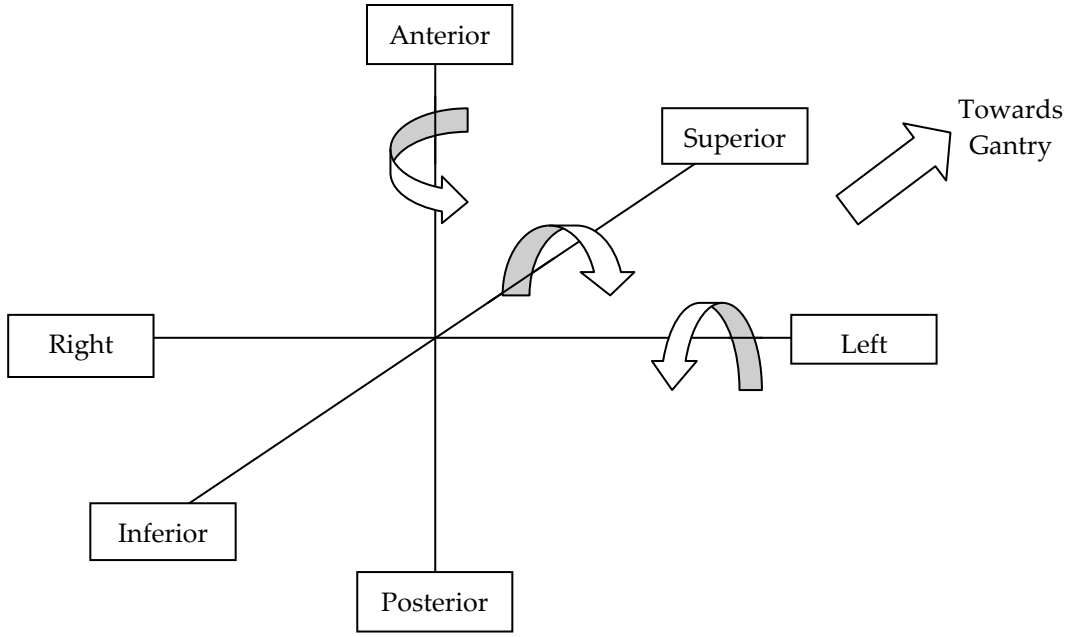

Figure 8: Diagram of the ELS rotational reference frame. The arrows indicate the direction of rotation that produces a positive rotation measurement by the ELS.

The geometric residual, rotational alignment and intertransponder distances for Patients 1 – 10 were tabulated and the trends in these measurements over a course of radiation therapy were characterized. The patient-specific causes of variations in the geometric residual, rotational alignment and intertransponder distances were investigated. We also determined whether the default maximum limits for the geometric residual (2 mm) and rotational alignment (10° in any direction) were appropriate for the majority of patients.

Two patients (Patients 3 and 8) exhibited the largest variation in geometric residual, intertransponder distances and rotational alignment over the course of radiation therapy and the data from these patients were further analyzed.

2.3 Motion Studies

To determine the feasibility of using the ELS in conjunction with intensity-modulated arc therapy treatments, the probability that a significant excursion would occur during the shorter treatment was investigated. Since corrections for displacements are only made during radiation delivery, not before or after, the continuous tracking data from the time of the first radiation beam-on to the end of the last radiation field for Patients 1 – 10 were used in the subsequent analysis. The frequency of excursions > 1 mm, > 2 mm, > 3 mm, > 4 mm and > 5 mm was determined for each patient using corrected and uncorrected tracking data. Corrected tracking data refer to the actual displacements that occurred during the treatment sessions, including any patient repositioning performed to reduce the magnitude of the displacements. Uncorrected tracking data refer to the displacements that would have occurred if treatment couch shifts had not been performed to reposition a patient during a treatment session. The magnitude of the treatment couch shifts is provided in the ELS session reports and this information was used to retrospectively "remove" (undo) any shifts and to simulate the prostate motion in the absence of any real-time repositioning.

In addition to quantifying the frequency of excursions occurring during an entire treatment session, the frequency of excursions was also determined for the first 120 seconds of the treatments. The data from the first 120 seconds of each treatment were used to better simulate the shorter treatment time of an IMAT session. The frequency of

excursions > 1 mm, > 2mm, > 3 mm, > 4 mm and > 5 mm was determined for each patient using the uncorrected motion data. The uncorrected motion data were used because the goal was to determine the probability of various excursions occurring when the patient was not repositioned. This better simulates an IMAT session because, as described previously, it is best to avoid interrupting the radiation delivery if possible.

Additionally, the maximum and minimum displacements occurring in each direction during the first 120 seconds of each patient's treatment were determined for each treatment session, for all patients. The data for the patients with the smallest and largest maximum and minimum displacements are presented to display the behavior of a very stable patient and a "worst case scenario" from our patient population. It illustrates the range of motion that was seen in our patient population during the first 120 seconds of treatment.

2.4 Margin Analysis

Appropriate planning margins based on the probability of target volume coverage were determined numerically using a formula developed by van Herk, et al[1]. This group used their recent data on the accuracy of prostate irradiation to derive "realistic" minimum dose-population histograms for different margins, assuming a homogenous dose distribution. As described previously, the formula used in this project was based on the requirement that the minimum dose to the CTV was 95% of the prescription dose or higher for 90% of the population[1]. van Herk, et al., fully separated

the geometrical deviations into systematic and random variations[1]. Typically, the standard deviation of various geometrical errors should be added in quadrature. However, the random and systematic components may result in different margins so van Herk, et al., added them linearly. Based on the minimum dose criteria used for the formula, the margin is created by first accounting for systematic errors to ensure a specified percentage coverage of the target. Then, a margin is added to account for the random errors to ensure coverage of the first margin up to a specified dose[23]. The margin equation is given as follows:

$$Margin = 2.5\,\Sigma + 0.7\,\sigma \tag{1}$$

Σ represents the standard deviation (SD) of the systematic error, while σ represents the standard deviation of the random error[23]. This formula was used to determine an appropriate margin for each patient individually (Patients 1 – 10) and for the population as a whole. Margins were determined in each direction (lateral, longitudinal and vertical) individually.

When using this formula to determine the margin for an individual patient, the average displacement for each fraction ($\bar{y}_{fx}$) and the standard deviation of the displacement for each fraction (σ_{fx}) was first determined. Then, Σ was found by computing the standard deviation of the average displacement over all fractions as follows.

$$\Sigma_{patient} = SD(\bar{y}_{fx}) \tag{2}$$

Next, σ was found by taking the root mean square (RMS) of the standard deviation of the displacement over all fractions and the values for Σ and σ were used in Equation 1 to compute the margin. The RMS in this case is equal to the square root of the mean of the squares of the standard deviation for all fractions.

$$\sigma_{patient} = RMS(\sigma_{fx}) \tag{3}$$

When using the margin formula for the population, the average displacement over the entire course of treatment ($\bar{y}_{tx}$), or systematic error, and the standard deviation of the displacement over the entire course of treatment (σ_{tx}), representing random error, was first calculated for each patient. Then, Σ was found by computing the standard deviation of the average displacement over the entire course of treatment for all patients, as follows.

$$\Sigma_{population} = SD(\bar{y}_{tx}) \tag{4}$$

Next, σ was found by taking the RMS of the standard deviation of the displacement over the entire course of treatment for each patient and the values for Σ and σ were used in Equation 1 to compute the population margin. The RMS in this case is equal to the square root of the mean of the squares of the standard deviation of displacement for each patient.

$$\sigma_{population} = RMS(\sigma_{tx}) \tag{5}$$

2.5 Dosimetric Analysis

The data from Patients 3 and 8 were used to evaluate the dosimetric impact of varying geometric residual, intertransponder distances and rotational alignment throughout a course of radiation therapy. These two patients were selected because both exhibited interesting and unique prostate deformations over the course of therapy (discussed in section 3.2). Patients 3 and 8 received weekly CBCT scans and the electromagnetic array was removed during image acquisition. For analysis, the prostate, rectum and bladder were contoured on these CBCT images. The prostate was contoured by the radiation oncologist and the completed contours of the rectum and bladder were evaluated by the physician and adjusted if necessary. The seminal vesicles could not be accurately contoured on the CBCT images and thus these were ignored during the subsequent analysis. Due to technical difficulties during the original imaging sequence, only 3 CBCT scans were available for Patient 3 while 6 CBCT scans were usable for Patient 8.

First, the delivered treatment plans (5 mm planning margin, primary and boost plans) were copied onto each CBCT scan for Patients 3 and 8, using the same monitor units (MUs)/field to mimic the actual treatment delivery. The MUs for each beam were standardized to confirm that the plans were copied and applied to the CBCT scans correctly. The prescription dose for both Patients 3 and 8 was 76 Gy. After calculating the dose on the CBCT scans using the original treatment plan, the impact of prostate

deformations was evaluated by comparing dosimetric indicators based on the planning CT and CBCT scans. The following points were evaluated:

1) Absolute volume of rectum receiving greater than or equal to 40 Gy, 60 Gy, 70 Gy and the prescription dose
2) Absolute volume of bladder receiving greater than or equal to 40 Gy, 60 Gy, 70 Gy and the prescription dose
3) Percentage volume of prostate receiving greater than or equal to 95% and 100% of the prescription dose
4) Minimum dose delivered to the prostate (delivered to 1 cm^3 volume)

The minimum dose delivered to the prostate is an important factor to evaluate because underdosage of the target strongly influences the tumor control probability[10].

After calculating dose on the CBCT scans using the original treatment plans (5 mm planning margin), a new plan utilizing a 3 mm planning margin was designed on the original planning CT scan and applied to the CBCT scans. To provide consistency and allow for better comparison, the new 3 mm plan was normalized to deliver 100% of the prescription dose to 95% of the PTV on the original planning CT scan. At this point (100% dose, 95% target coverage), the prostate dose-volume histograms (DVHs) for the 3 mm plan and the original plan were equivalent. The same dosimetric indicators as described above were used to compare the DVHs for the planning CT and CBCT scan based on the 3 mm plan. A 3 mm margin was tested since this margin was found to be

suitable for the majority of patients using the corrected motion data in the formula developed by van Herk et al[1]. The margins generated from the corrected motion data (as opposed to uncorrected motion data) were used because we wanted to determine if a smaller margin would be suitable for future ELS patients, for whom repositioning could be performed.

To confirm that any difference in prostate coverage, bladder dose or rectal dose for Patient 8 was due to target rotation instead of an alignment error, any displacements of the patient's anatomy from the reference position were removed for each CBCT scan prior to calculating the dose distribution. The displacements of the anatomy, if any, were determined using Offline Review software as described in Section 2.1. These displacements were removed by shifting the treatment isocenter with respect to the patient.

3. Results

3.1 Electromagnetic Localization System Accuracy Verification

Small but statistically significant differences between the planar and CBCT measured alignments and the electromagnetic alignments were observed. The hypothesized mean difference at which the electromagnetic and planar image alignments for the population were indistinguishable based on the student's paired t-test ($p > 0.05$) was 0.6 mm in the AP direction and 0.1 mm in the SI and RL directions. The hypothesized mean difference at which the electromagnetic and CBCT alignments for the population were indistinguishable was 1.0 mm in the AP direction, 0.1 mm in the SI direction and 0.25 mm in the RL direction. These values are displayed for each patient and for the population in Table 1, below.

Table 1: Hypothesized mean difference between the electromagnetic and planar/CBCT alignments at which the populations were indistinguishable.

Hypothesized Mean Difference (mm)- Planar			
Patient	AP (Vertical)	SI (Longitudinal)	RL (Lateral)
1	0.5	0.25	0.25
2	0.25	0.75	0.5
3	1.25	0.5	0.25
4	0.25	0.25	0.5
5	0.5	0.25	0.0
7	0.5	0.25	0.0
8	0.0	0.25	0.75
9	1.0	0.5	0.25
10	0.25	0.25	0.25
Population	0.6	0.1	0.1
Hypothesized Mean Difference (mm)- CBCT			
Population	1.0	0.1	0.25

3.2 Positional and Rotational Reproducibility of Transponders

Several patients exhibited large rotations that exceeded the default maximum limit set by the ELS. Other patients showed a steady decrease in intertransponder distances over the course of treatment, while the remaining patients exhibited steady intertransponder distances and only small rotations.

3.2.1 Geometric Residual

The population geometric residual was 0.8 ± 0.4 mm. For individual patients, the largest daily geometric residual was 1.4 mm (Patient 10), while the largest standard deviation was 0.3 mm (Patient 2). The default maximum limit of 2 mm for geometric residual was never exceeded in our patient population. The mean and standard

deviation of the geometric residual for each patient and the population are displayed below in Table 2.

Table 2: Mean and Standard Deviation of the Geometric Residual

Geometric Residual		
Patient	Mean (mm)	SD (mm)
1	0.2	0.1
2	1.0	0.3
3	0.5	0.3
4	0.9	0.2
5	0.4	0.1
6	0.3	0.1
7	0.9	0.2
8	1.3	0.2
9	0.9	0.2
10	1.4	0.2
Population	0.8	0.4

3.2.2 Rotational Alignment

Setup rotations had the greatest magnitude and uncertainty in pitch (about the lateral axis, -3.1° ± 6.4°) while roll (longitudinal axis, 0.2° ± 3.0°) and yaw (vertical axis, 0.2° ± 3.1°) were smaller and more consistent. The default maximum rotational limit of 10° in each axis has been exceeded in multiple patients during multiple treatment sessions. No results are available for Patient 1 because only 2 transponders were available for that patient's daily alignment.

Table 3: Mean and Standard Deviation of the Rotational Alignment about the Lateral, Longitudinal and Vertical Axes

Rotational Alignment						
	Pitch (Lateral axis)		Roll (Longitudinal axis)		Yaw (Vertical axis)	
Patient	Mean	SD	Mean	SD	Mean	SD
2	-7.0°	1.8°	-2.7°	1.7°	1.3°	0.6°
3	0.4°	3.1°	0.8°	0.9°	-1.4°	0.9°
4	-5.1°	4.4°	-2.0°	0.9°	2.7°	0.8°
5	1.6°	4.4°	-1.0°	1.6°	1.2°	0.6°
6	-5.9°	4.7°	-0.2°	2.0°	0.9°	1.5°
7	0.0°	8.3°	-2.5°	2.1°	0.5°	1.3°
8	-10.1°	6.9°	5.8°	1.9°	-6.7°	2.2°
9	2.3°	3.5°	1.4°	1.1°	0.0°	2.0°
10	-5.0°	3.1°	1.6°	1.7°	3.6°	1.4°
Population	-3.1°	6.4°	0.2°	3.0°	0.2°	3.1°

Patient 8 had the largest average rotational displacement (up to 23.2°), possibly due to one transponder being located next to the prostate-rectum interface which may have caused the position of this transponder to be very susceptible to variations in rectal filling. The rotational alignment over the course of radiation therapy for Patient 8 is displayed in Figure 9, below.

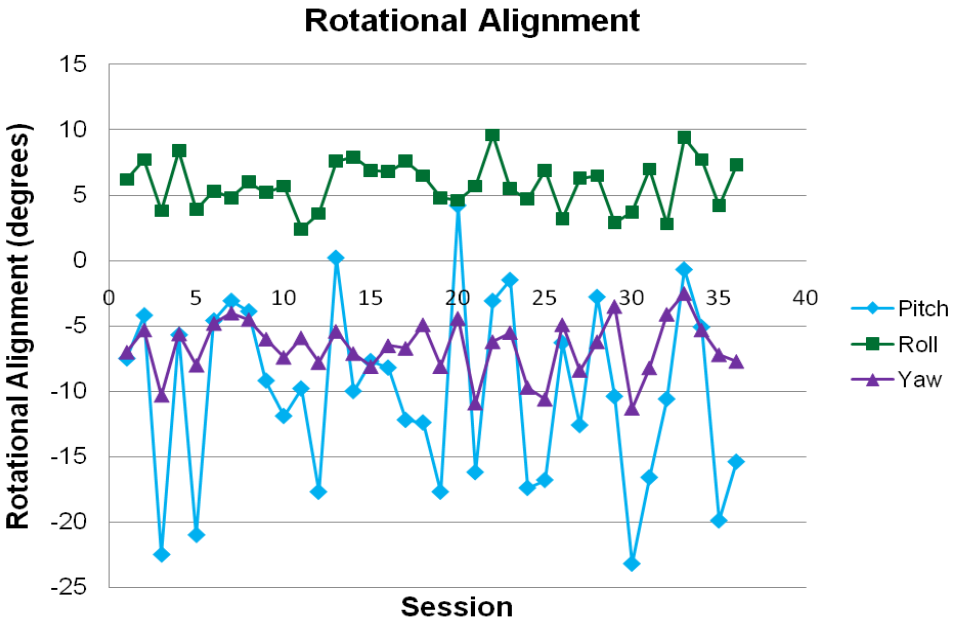

Figure 9: Patient 8 Rotational Alignment about the Lateral, Longitudinal and Vertical Axes

An axial CBCT image displaying the left transponder is shown in Figure 10 to illustrate its close proximity to the rectum.

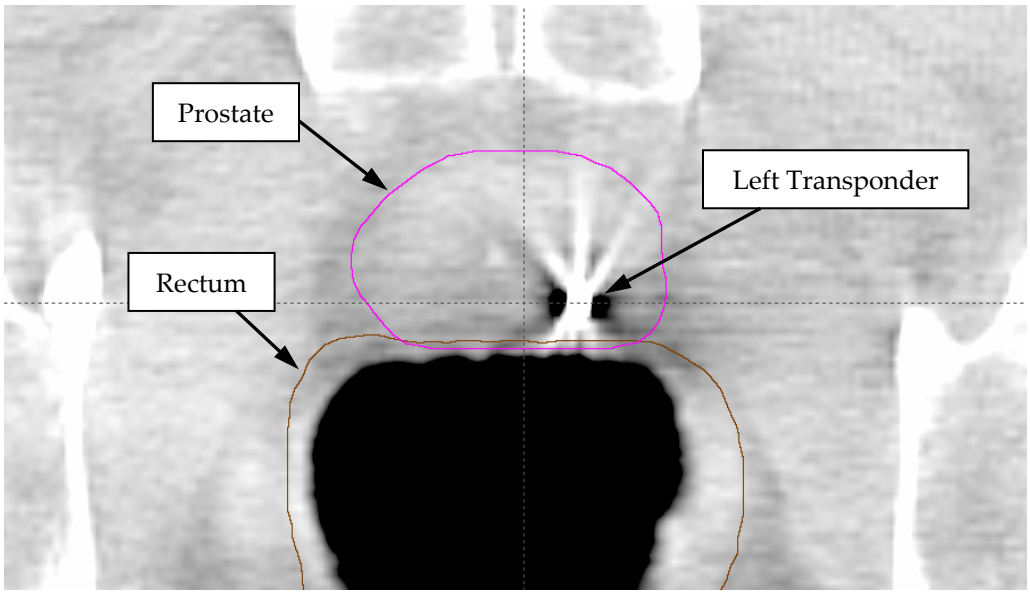

Figure 10: Axial CBCT image of the prostate and rectum. The left transponder is located in the prostate and adjacent to the rectum, as indicated by the arrow.

Figure 11 and Figure 12 (zoomed-in version), below, are sagittal CBCT images of the left transponder to again demonstrate the position of the transponder within the prostate in relation to the rectum. Figure 12 also displays the distances between each transponder center, as measured from this sagittal slice.

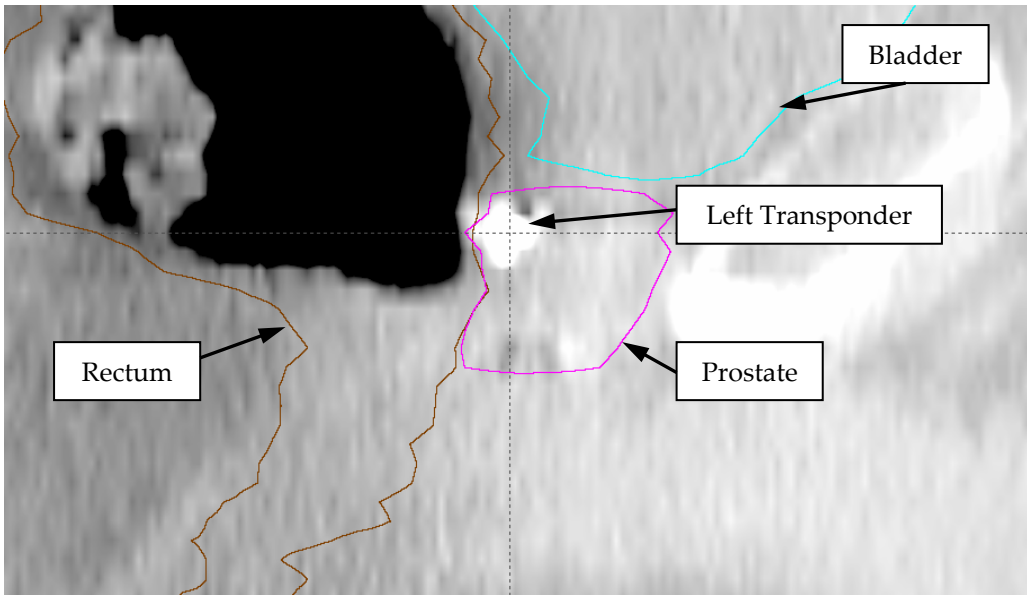

Figure 11: Sagittal CBCT image of the prostate, rectum and bladder. The position of the left transponder is indicated by the arrow. See Figure 12 for a zoomed-in view.

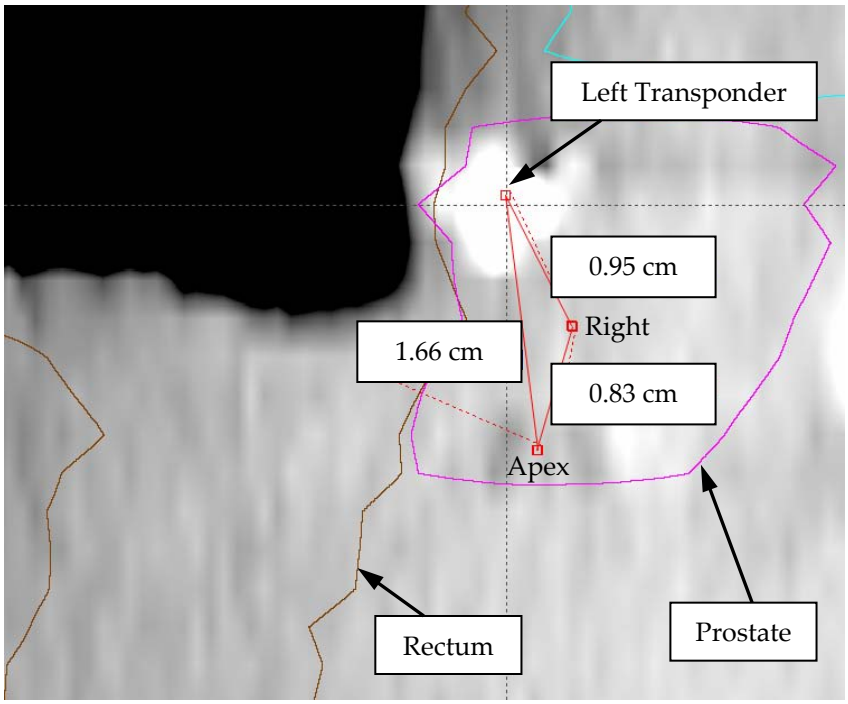

Figure 12: Zoomed-in sagittal CBCT image of the prostate and rectum. The position of the left transponder is indicated by the arrow and the center of the apex and right transponder (measured vertically and longitudinally) are also displayed. The distance between each transponder center is displayed (indicated by the red lines forming a triangle).

3.2.3 Intertransponder Distances

Several trends were seen in the measured intertransponder distances over the course of treatment. First, some patients exhibited essentially no change. Other patients had significant decreases (roughly 2 – 3 mm) in intertransponder distances over the eight weeks of radiation therapy (Patient 2 and Patient 3), possibly due to prostate shrinkage (see section 3.5.1). The change in intertransponder distances caused their geometric residuals to increase steadily. Representative data for Patient 3 are displayed below in Figure 13 and Figure 14. Figure 13 displays the difference between the

measured and planned intertransponder distances as the course of therapy progresses. It is obvious that after treatment session 12, all three intertransponder distances for Patient 3 decrease steadily. As indicated in Figure 14, the geometric residual, which depends on the transponder configurations for each treatment session as compared to the planning CT, increases as the intertransponder distances change.

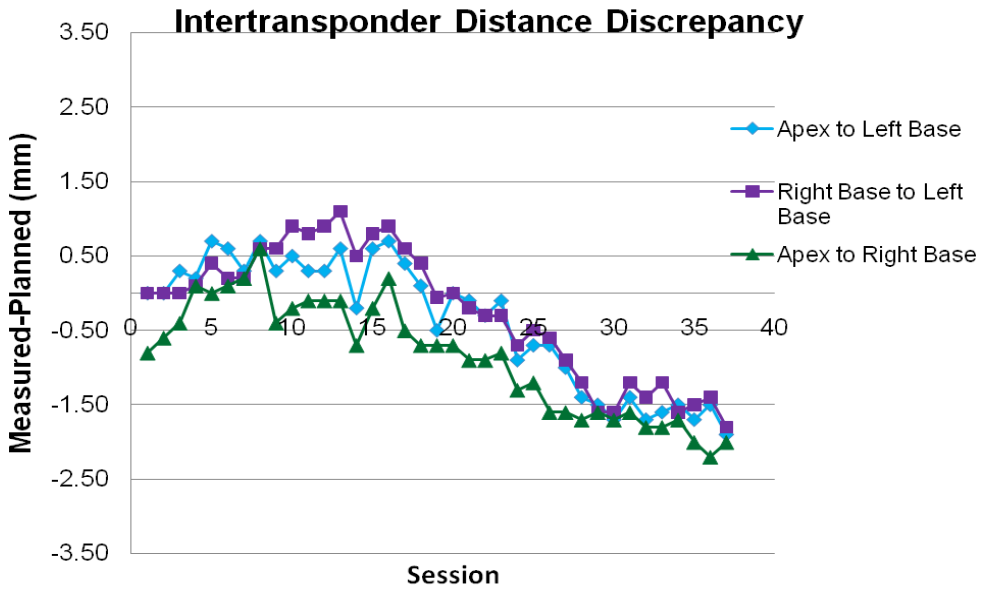

Figure 13: Patient 3 Intertransponder Distance Discrepancy

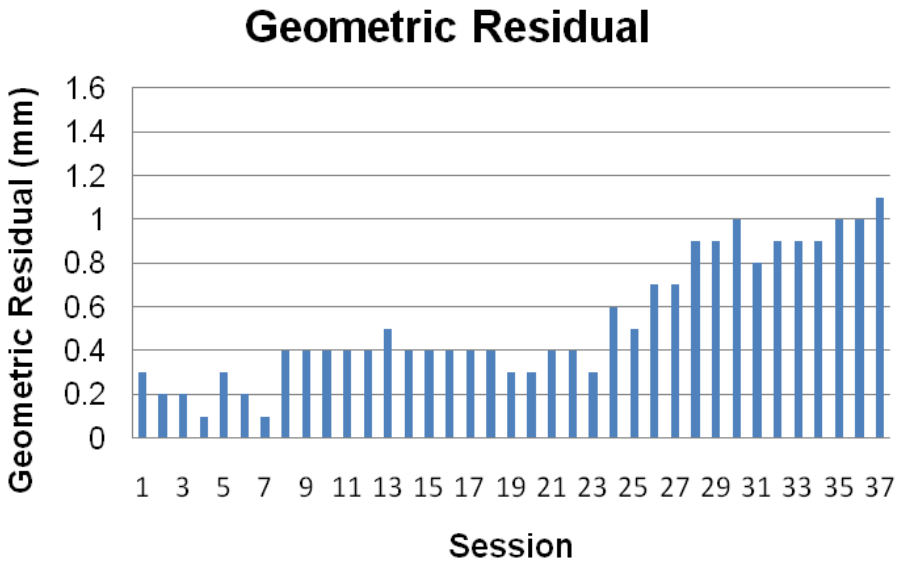

Figure 14: Patient 3 Geometric Residual

The third trend showed large differences between intertransponder distances measured for all treatment sessions as compared to those from the planning CT (Patient 8). These discrepancies imply that the transponder geometry acquired for treatment planning was not representative of the day-to-day geometry during treatment. This systematic error may be due to the transponder implant location. Patient 8 also exhibited up to a 2 mm variation in the Apex-to-Left Base intertransponder distance between treatment sessions, as indicated in Figure 15. The geometric residual for Patient 8 was large compared to other patients but remained fairly steady over the course of radiation therapy, as indicated in Figure 16.

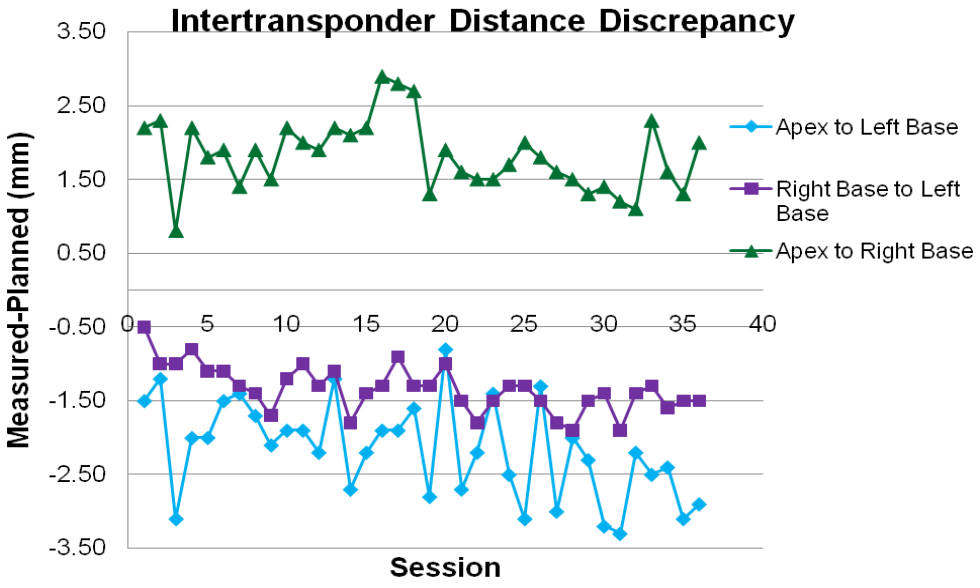

Figure 15: Patient 8 Intertransponder Distance Discrepancy

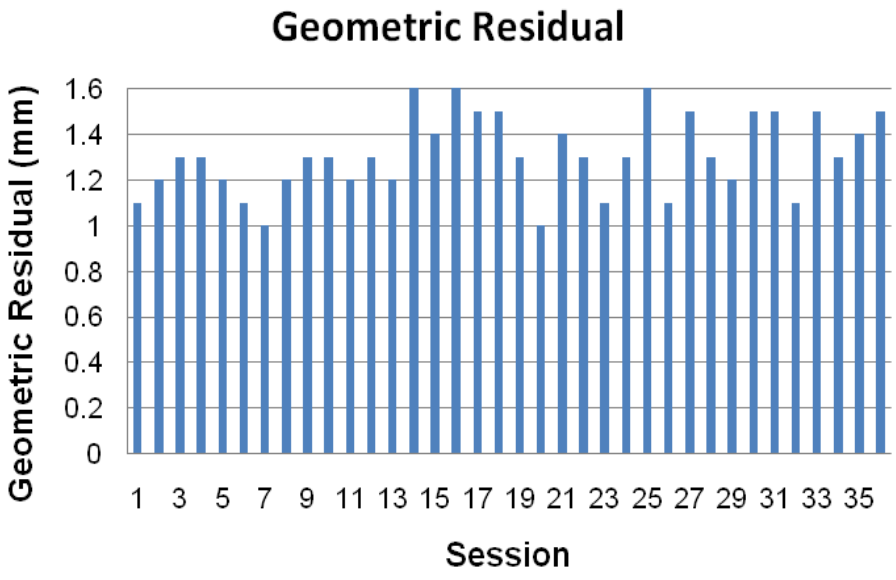

Figure 16: Patient 8 Geometric Residual

3.3 Motion Studies

3.3.1 Excursion Frequency During Entire Treatment

The frequency of excursions > 1 mm, > 2 mm, > 3 mm, > 4 mm and > 5 mm occurring during a treatment session was determined for each patient using corrected and uncorrected motion data. These data are presented for each patient in the lateral, longitudinal and vertical directions. The frequency of the uncorrected lateral, longitudinal and vertical target excursions is displayed in Figure 17, Figure 19 and Figure 21, respectively. The frequency of the corrected lateral, longitudinal and vertical target excursions is displayed in Figure 18, Figure 20 and Figure 22, respectively. These data are also presented in tabular form in Appendix A. It is obvious from these figures that the frequency of excursions > 3 mm, > 4 mm and > 5 mm is greater when the uncorrected motion data are evaluated. The frequency of excursions > 1 mm and > 2 mm is nearly equivalent for the corrected and uncorrected motion data because the radiation therapists were instructed to reposition the patient when an excursion exceeded 3 mm. The charts indicate that the most excursions occur in the AP direction, with the least excursions occurring in the lateral direction. The majority of excursions occurring in the lateral direction are less than 3 mm while the majority of excursions in the vertical direction are less than 5 mm, when considering the uncorrected motion data.

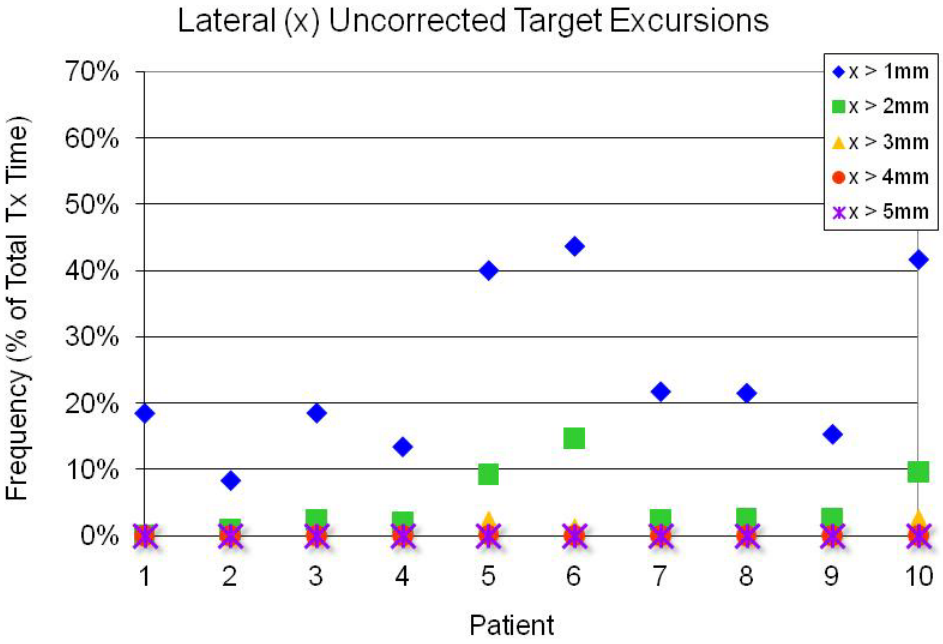

Figure 17: Frequency of lateral uncorrected target excursions during the entire treatment session.

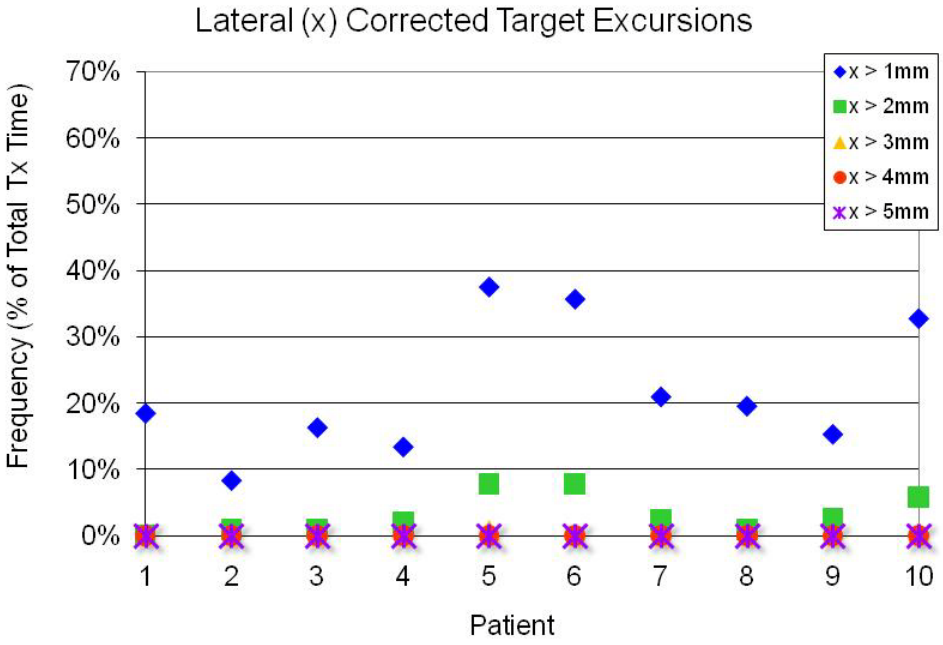

Figure 18: Frequency of lateral corrected target excursions during the entire treatment session.

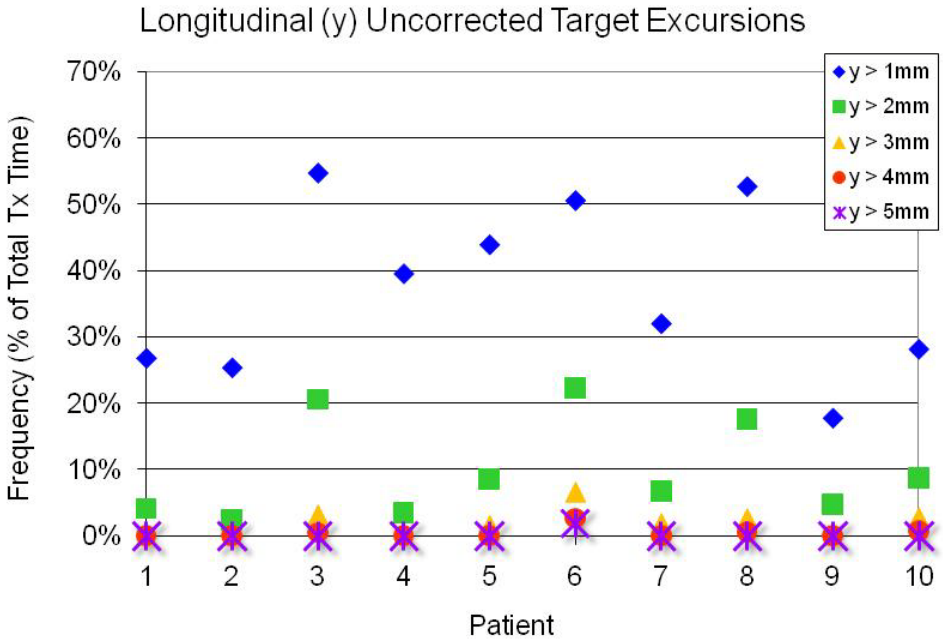

Figure 19: Frequency of longitudinal uncorrected target excursions during the entire treatment session.

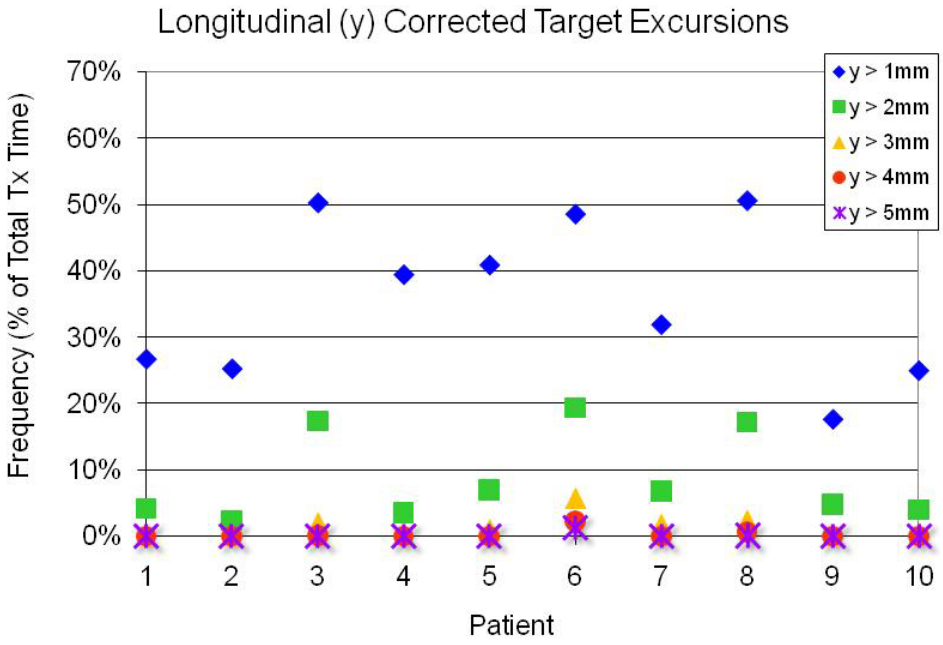

Figure 20: Frequency of longitudinal corrected target excursions during the entire treatment session.

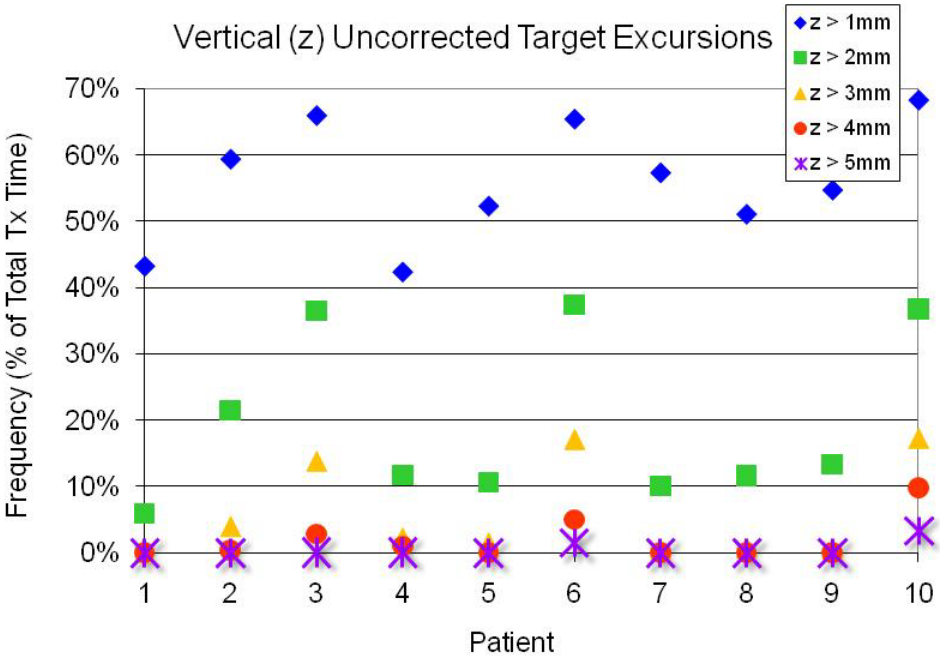

Figure 21: Frequency of vertical uncorrected target excursions during the entire treatment session.

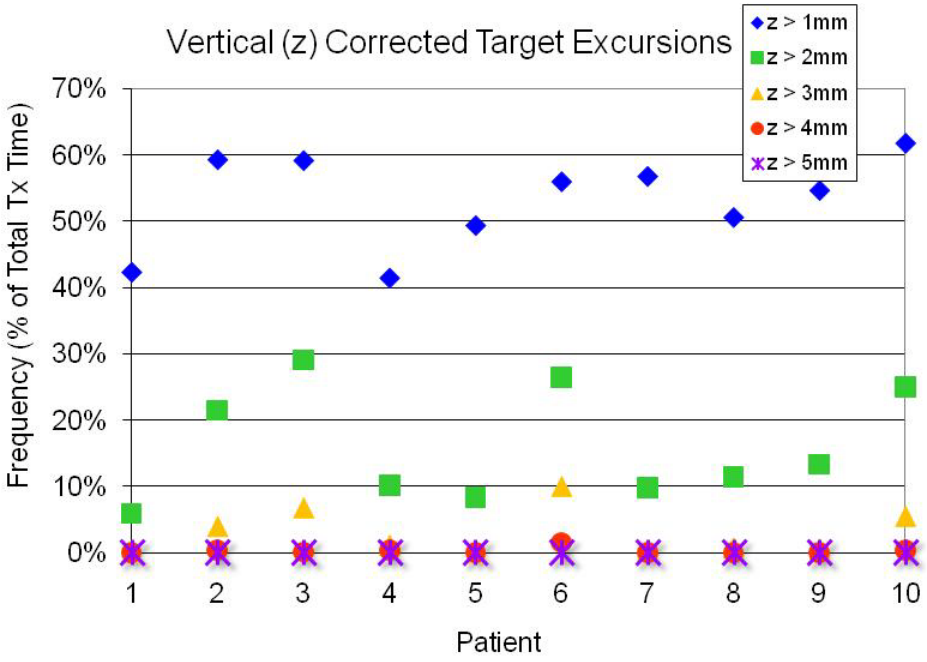

Figure 22: Frequency of vertical corrected target excursions during the entire treatment session.

3.3.2 Excursion Frequency During First 120 Seconds of Treatment

In addition to quantifying the frequency of excursions occurring during an entire treatment session, the frequency of excursions was also determined for the first 120 seconds of the treatments to simulate an IMAT treatment session. The frequency of excursions > 1 mm, > 2 mm, > 3 mm, > 4 mm and > 5 mm was determined for each patient using the uncorrected motion data and this information is displayed in Figure 23, Figure 24 and Figure 25 for the lateral, longitudinal and vertical directions, respectively. These data are also presented in tabular form in Appendix A. It can be noted that the frequency of excursions occurring during the first 120 seconds of treatment is much less than when considering the entire treatment session. The majority of excursions occurring in the lateral and longitudinal directions are less than 3 mm while the majority of excursions are less than 4 mm in the vertical direction.

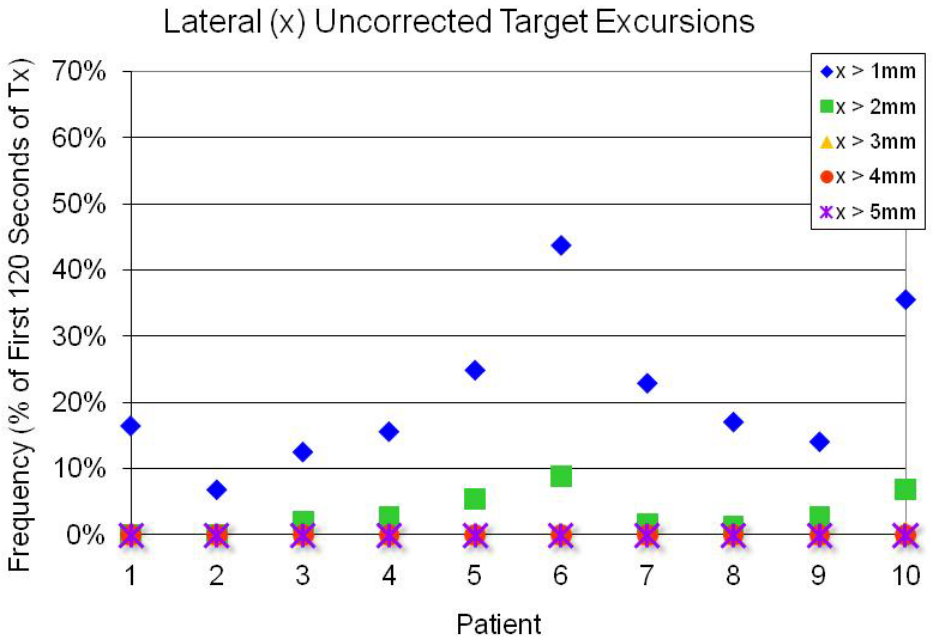

Figure 23: Frequency of lateral uncorrected target excursions during the first 120 seconds of the treatment session.

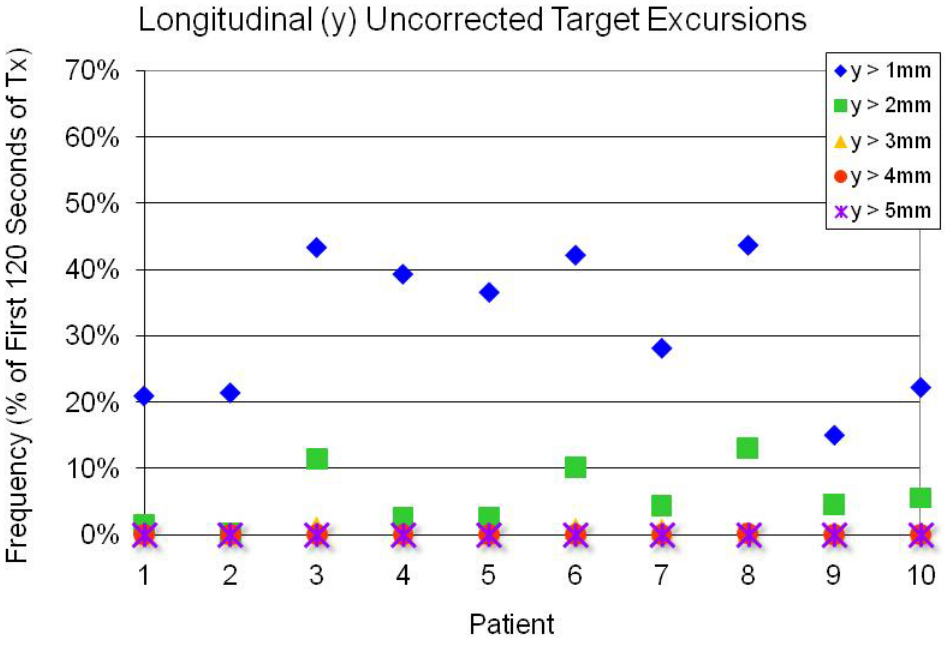

Figure 24: Frequency of longitudinal uncorrected target excursions during the first 120 seconds of the treatment session.

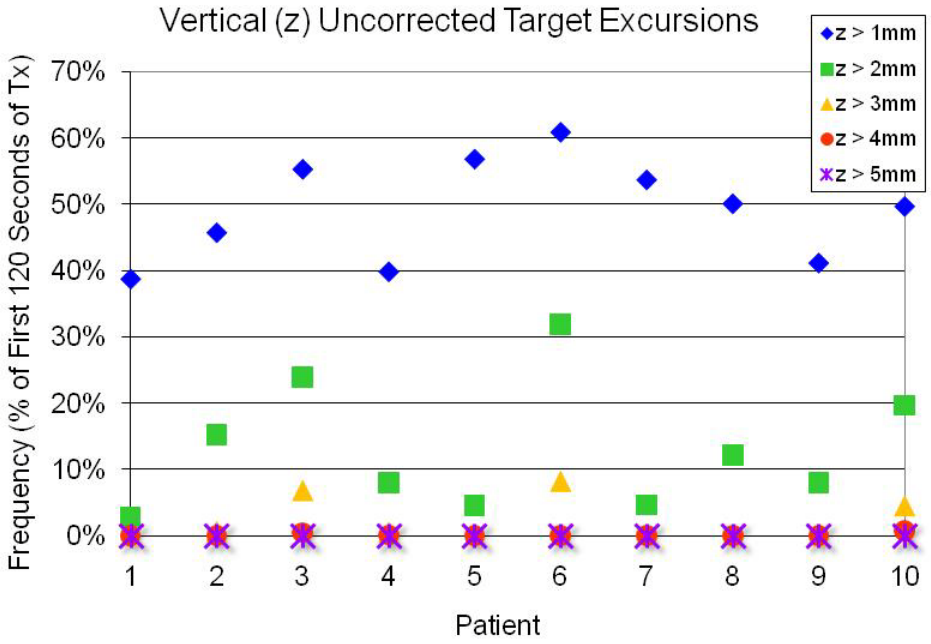

Figure 25: Frequency of vertical uncorrected target excursions during the first 120 seconds of the treatment session.

3.3.3 Range of Motion During First 120 Seconds of Treatment

In addition to evaluating the frequency of target excursions occurring during an entire treatment session and during the first 120 seconds of a treatment session, the range of motion occurring in each direction during the first 120 seconds of treatment is presented for Patients 1 and 3 in Figure 26 and Figure 27. These figures display the maximum and minimum displacement occurring during the first 120 seconds of each treatment session. Patient 1 displayed some of the smallest maximum and minimum displacements while Patient 3 displayed some of the largest maximum and minimum displacements from our patient population. Patient 3 represents an example of the worst case scenario (from our patient population) in terms of displacements that could occur

during an IMAT treatment. Even for Patient 3, all excursions, except for one (-5.05 mm) in the vertical direction, were less than 5 mm.

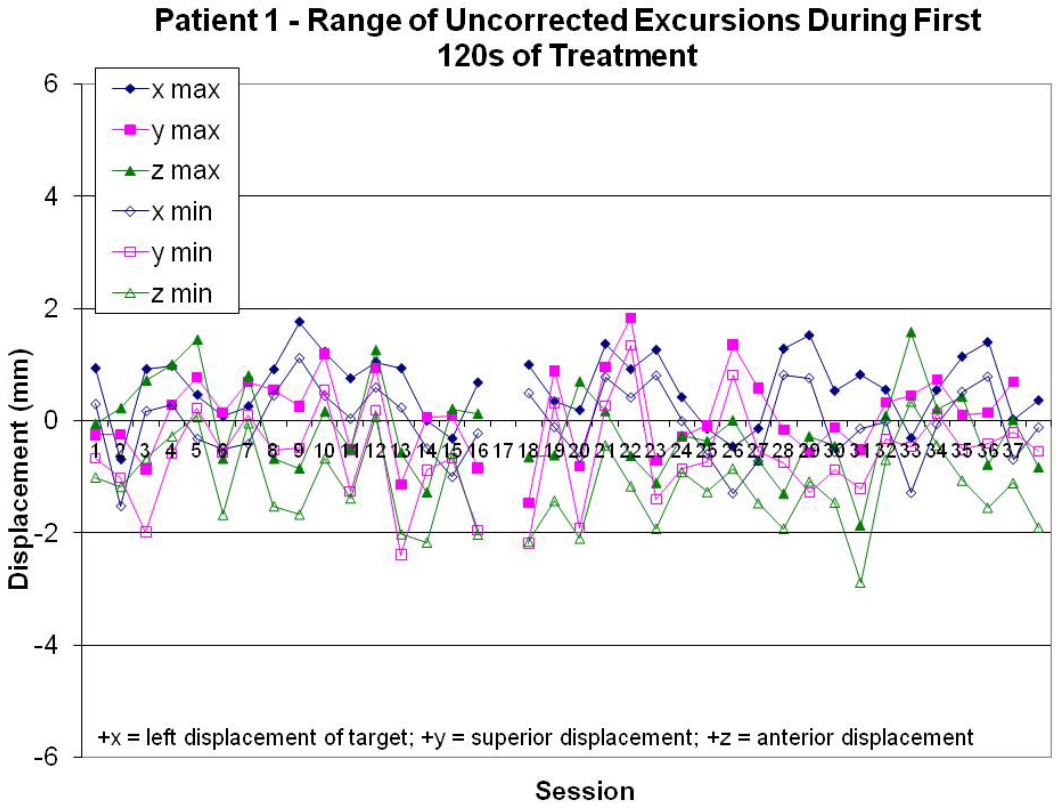

Figure 26: Patient 1 range of uncorrected target excursions during first 120 seconds of the treatment session.

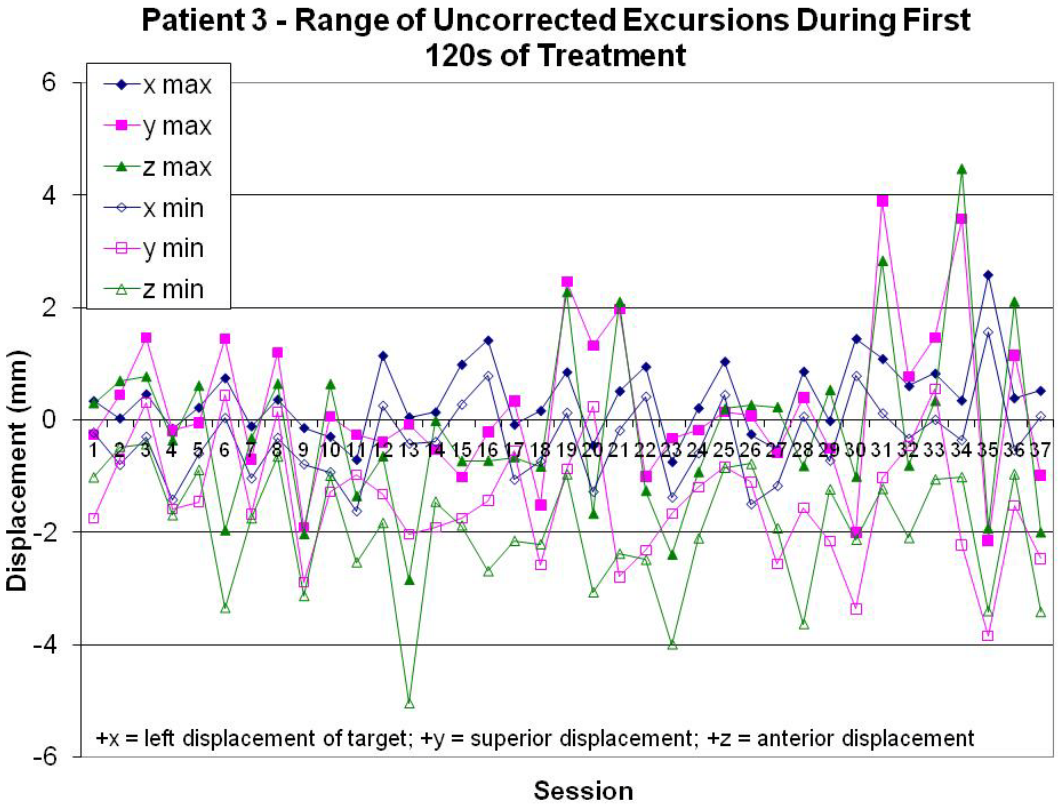

Figure 27: Patient 3 range of uncorrected target excursions during first 120 seconds of the treatment session.

3.4 Margin Analysis

Using a formula developed by van Herk, et al., appropriate treatment margins were computed to satisfy the requirement that the minimum dose delivered to the CTV was 95% of the prescription dose or higher for 90 % of the population[1]. Both corrected and uncorrected motion data were used as input to the margin formula. The margins generated based on the corrected and uncorrected motion data are presented in Table 4 and Table 5, respectively. Margins were generated for each patient individually and for the population. The population margins using the corrected motion data were 1.24 mm,

1.96 mm and 1.57 mm in the lateral, longitudinal and vertical directions, respectively. The population margins using the uncorrected motion data were 1.42 mm, 2.08 mm and 1.97 mm in the lateral, longitudinal and vertical directions, respectively.

The generated margins for individual patients and the population were largest in the longitudinal and vertical directions. The margins were larger using the uncorrected data because this motion data includes more displacements. The margins generated using the corrected motion data were less than 3 mm for the population analysis and for all patients except Patient 6 in the longitudinal direction and Patient 8 in the longitudinal and vertical directions. The margins generated using the corrected motion data were always less than 4 mm. Even using the uncorrected motion data, the margins were less than 3 mm for the population and all patients in the lateral direction. The margin was greater than 3 mm for Patients 6 and 8 in the longitudinal direction and for Patients 3, 5, 6, 8, and 10 in the vertical direction. During the dosimetric analysis, an isotropic 3 mm margin was tested since this margin was found to be suitable for the majority of patients when the corrected motion data were used in the margin formula.

Table 4: Lateral, Longitudinal and Vertical Margins Generated using Corrected Motion Data

Corrected			
Patient	Lateral (mm)	Longitudinal (mm)	Vertical (mm)
1	1.71	2.29	2.40
2	1.67	1.94	2.90
3	1.92	2.67	2.53
4	1.92	2.31	2.36
5	2.05	2.80	2.93
6	2.20	3.60	2.93
7	1.96	2.46	2.01
8	1.86	3.13	3.05
9	1.81	2.03	1.91
10	2.15	2.20	2.62
Population	1.24	1.96	1.57

Table 5: Lateral, Longitudinal and Vertical Margins Generated using Uncorrected Motion Data

Uncorrected			
Patient	Lateral (mm)	Longitudinal (mm)	Vertical (mm)
1	1.71	2.29	2.40
2	1.67	1.94	2.90
3	2.10	2.91	3.33
4	1.92	2.31	2.57
5	2.27	3.08	3.25
6	2.55	4.02	3.68
7	1.98	2.48	2.02
8	2.12	3.31	3.22
9	1.81	2.03	1.91
10	2.49	2.76	3.89
Population	1.42	2.08	1.97

3.5 Dosimetric Analysis

The following points were evaluated to compare the DVHs resulting from the application of the 3 mm and 5 mm margin (original) treatment plans to the planning CT scan as well as to the CBCT scans for Patients 3 and 8:

1) Absolute volume of rectum receiving greater than or equal to 40 Gy, 60 Gy, 70 Gy and the prescription dose
2) Absolute volume of bladder receiving greater than or equal to 40 Gy, 60 Gy, 70 Gy and the prescription dose
3) Percentage volume of prostate receiving greater than or equal to 95% and 100% of the prescription dose
4) Minimum dose delivered to the prostate (delivered to 1 cm^3 volume)

The dosimetric indicators for the planning CT and CBCT scans were plotted against the geometric residual and rotational alignment, respectively, for Patients 3 and 8 for the original 5 mm treatment plan. This allowed us to evaluate the differences, if any, in prostate coverage, rectal dose and bladder dose due to prostate deformations over the course of therapy and to discern any noticeable trends in the data.

Similar to the 5 mm treatment plan, the dosimetric indicators for the 3 mm treatment plan calculated on the planning CT and CBCT scans were plotted against the geometric residual and rotational alignment, for Patients 3 and 8, respectively, to

determine the difference in prostate coverage, rectal dose and bladder dose given a smaller planning margin.

Additionally, the absolute volumes of the prostate, rectum and bladder on the planning CT and CBCT scans were recorded and displayed to show the variation, if any, over the course of radiation therapy.

3.5.1 Patient 3

The dosimetric indicators for the three CBCT scans and planning CT scan were plotted against the geometric residual as measured during the treatment session at which the scan was acquired for Patient 3. The geometric residual and rotational alignment occurring during each of these treatment sessions is presented below in Table 6. The elapsed days from the first treatment session to the day of the CBCT scan are also recorded for each scan. The geometric residual increases over the course of treatment for Patient 3, so in the subsequent figures when the dosimetric indicators are plotted against the geometric residual, they are also plotted in chronological order.

Table 6: Patient 3 Geometric Residual and Rotational Alignment during the treatment session at which the planning CT and CBCT scans were acquired.

	Elapsed Days	Geometric Residual (mm)	Rotation		
			Pitch	Roll	Yaw
Planning CT	0	0.0	0°	0°	0°
CBCT 1	14	0.4	2°	1.2°	-0.5°
CBCT 2	24	0.5	-2.4°	2.6°	-1.1°
CBCT 3	34	1.0	-2.6°	0.8°	-2.5°

The bladder, rectum and prostate volumes are plotted against the elapsed treatment days in Figure 28, below. These volumes were determined in the treatment planning software based on the contours of the bladder, rectum and prostate on the planning CT and CBCT scans. This figure indicates the dramatic bladder volume variation and a fairly steady rectum volume. It also displays a decrease in the volume of the prostate over the course of treatment. The prostate volume decreases by roughly 20% from the planning CT scan (0 mm geometric residual) to the last CBCT scan (1 mm geometric residual) which supports our previous hypothesis of prostate shrinkage.

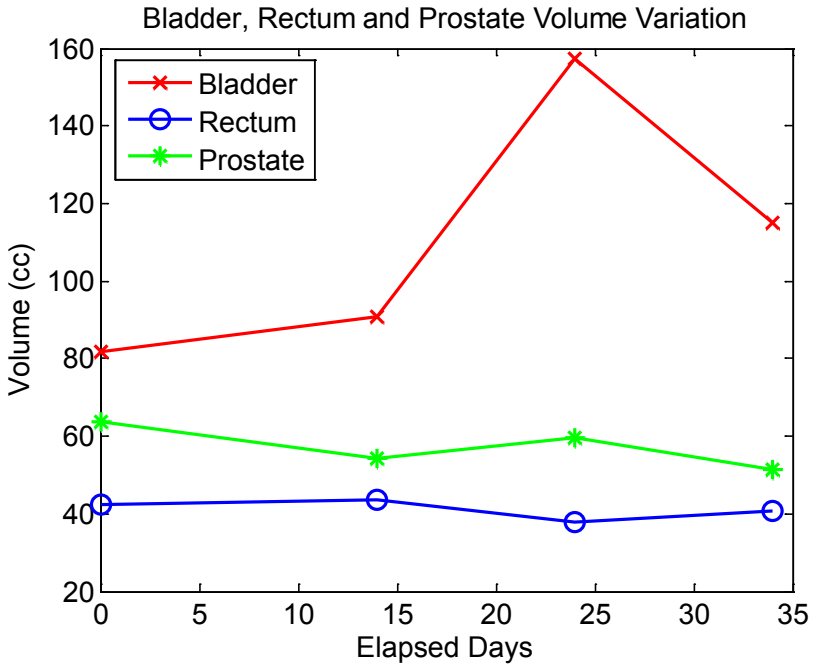

Figure 28: Patient 3 Bladder, Rectum and Prostate volumes measured from the planning CT and CBCT scans and displayed as a function of elapsed days.

In the next figure (Figure 29), the dosimetric indicators for the prostate as a function of the geometric residual are displayed. Each point on the chart represents a

dosimetric indicator for one of the four scans. The figure shows both the variation of prostate dose with geometric residual as well as the variation of prostate dose with a decreased planning margin. The prostate dosimetric indicators vary insignificantly with the geometric residual. The percentage volume receiving greater than or equal to 100% of the prescription dose is slightly lower (up to roughly 1% lower) for the 3 mm plan as compared to the 5 mm plan during two of the treatment sessions. There is an even smaller difference (up to roughly 0.3% difference) between the 5 mm and 3 mm plans when considering the lower dosimetric indicator (95% of the prescription dose) for these two treatment sessions. These small differences between the prostate coverage from the 5 mm and 3 mm plans are most likely clinically insignificant.

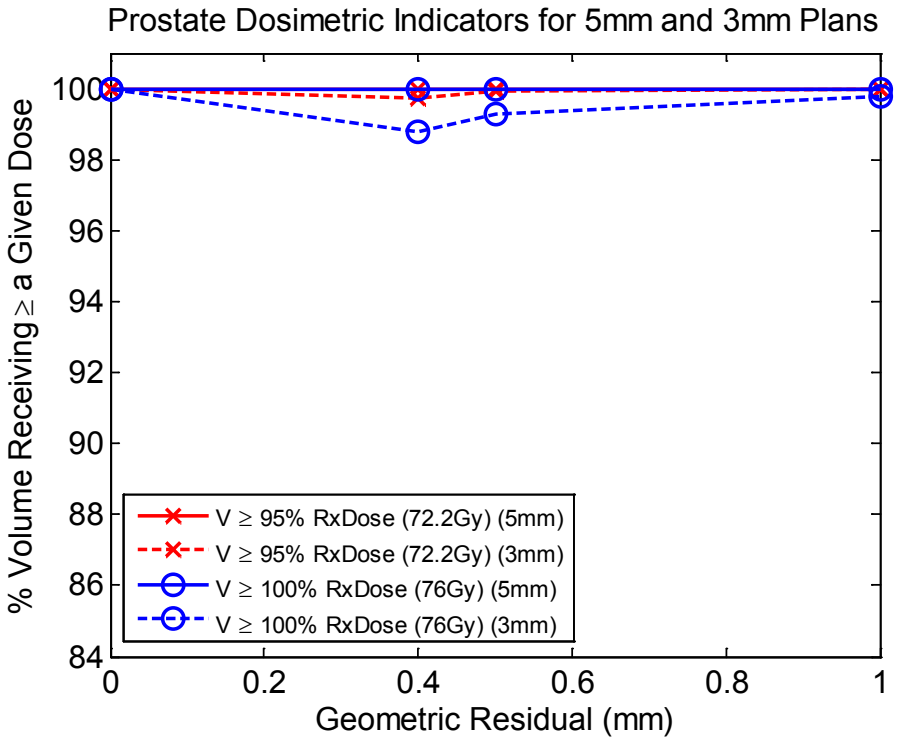

Figure 29: Patient 3 Prostate Dosimetric Indicator variation with geometric residual for 5 mm and 3 mm treatment plans.

Table 7, below displays the minimum dose delivered to the prostate from the 3 mm and 5 mm treatment plans as calculated on the planning CT and three CBCT scans. The elapsed days between a given scan and the first treatment session, as well as the geometric residual and rotational alignment, are displayed for clarity. The largest difference in the minimum prostate dose for the 5 mm and 3 mm treatment plans was 1.5% for the first CBCT scan. Similar to the results seen in Figure 29, the minimum prostate doses displayed in Table 7 seem to indicate an insignificant difference between the 5 mm and 3 mm treatment plans in terms of prostate coverage.

Table 7: Patient 3 Minimum Dose to the Prostate

	Elapsed Days	Minimum Prostate Dose (Gy) (1cc)		Geometric Residual (mm)	Rotation		
		5 mm Margin	3 mm Margin		Pitch	Roll	Yaw
Planning CT	0	77.4	77.1	0.0	0°	0°	0°
CBCT 1	14	77.8	76.6	0.4	2°	1.2°	-0.5°
CBCT 2	24	77.5	76.7	0.5	-2.4°	2.6°	-1.1°
CBCT 3	34	77.4	76.7	1.0	-2.6°	0.8°	-2.5°

The dosimetric data for the rectum and bladder are presented below in Figure 30 and Figure 31, respectively. The first chart includes the dosimetric indicators for the rectum while the second chart displays the analogous information for the bladder. The first data point on both charts corresponds to the planning CT scan, where the geometric residual is zero because this scan captures the reference positions of the transponders. Similar to the figure displaying the prostate dosimetric indicators, each point on the chart represents a dosimetric indicator for one of the four scans. The purpose of each chart is twofold. First, they display the variation of rectum or bladder dose with geometric residual. Second, they display the variation of rectum or bladder dose when a decreased planning margin is used. The rectum and bladder dose is quantified in terms of absolute volumes receiving greater than or equal to a given dose. We chose to use absolute volumes because we were most interested in what volume of each organ extended into the treatment field, and the often dramatic volume changes of the rectum

and bladder can result from expansion outside of the treatment field. If relative volumes were used, a large expansion outside of the treatment field may falsely alter the results.

There appears to be no clear trend between the rectum dose and geometric residual. In terms of the treatment plan comparison, there was a higher dose delivered to the rectum for the 5 mm plans as compared to the 3 mm plans, and this was more significant at the lower dose levels. It is more significant at the lower dose levels because the lower dose region is closest to the rectum. At the lowest dose level (40 Gy) there is a roughly 5 cm^3 (cc) difference between the volume receiving greater than or equal to 40 Gy between the 5 mm and 3 mm plans. This difference decreases to roughly 2 cc for the highest dose level (76 Gy). This difference may or may not cause clinically observable results for this patient.

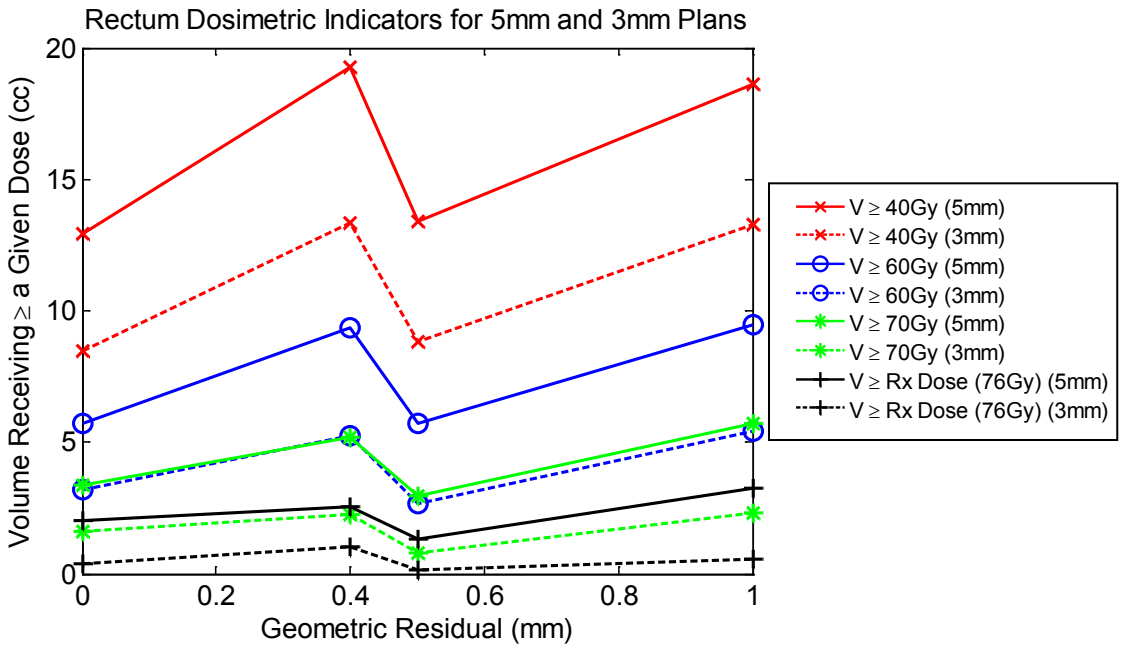

Figure 30: Patient 3 Rectum Dosimetric Indicator variation with geometric residual for 5 mm and 3 mm treatment plans.

As illustrated by Figure 31, below, there does not seem to be a strong trend between the bladder dose and the geometric residual. We might have expected the bladder and rectum dose to increase with geometric residual, since we hypothesized that the prostate was shrinking (and causing the increase in geometric residual), which may also have increased the volume of rectum and bladder within the field. The results for both the rectum and bladder suggest that this did not occur. It is obvious from the figure that the bladder receives a higher dose from the 5 mm plan than from the 3 mm plan at each dose level. At the lowest dose level (40 Gy), there is a roughly 12 – 14 cc difference between the volume receiving greater than or equal to 40 Gy from the 5 mm and 3 mm plans and this difference decreases to roughly 6 cc for the highest dose level

(76 Gy). As with the change in rectum dose, these small dose changes for the bladder may not be clinically significant.

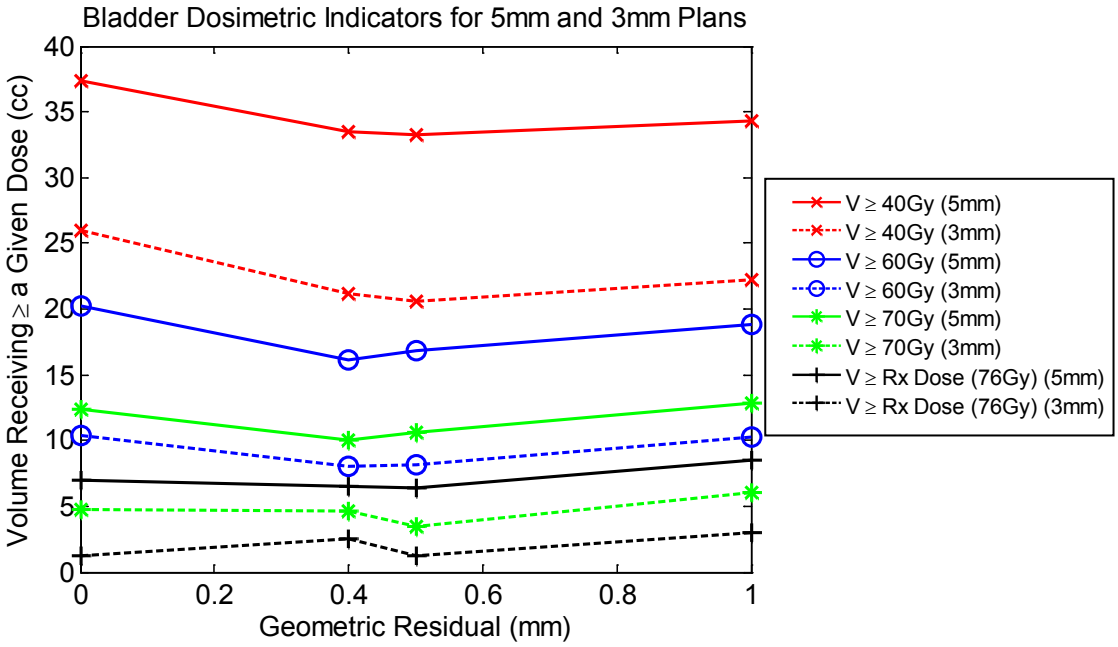

Figure 31: Patient 3 Bladder Dosimetric Indicator variation with geometric residual for 5 mm and 3 mm treatment plans.

3.5.2 Patient 8

The dosimetric indicators for the six CBCT scans and planning CT scan were plotted against the daily target rotation for Patient 8. The geometric residual and rotational alignment occurring during each of these treatment sessions is presented below in Table 8, in addition to the elapsed days from the first treatment session to the day of each subsequent scan. The rotational alignment exhibited the largest magnitude in pitch and the smallest magnitude in roll. It is interesting to note that the rotation

about each axis for Patient 8 was generally consistent in the direction of rotation during the course of therapy.

Table 8: Patient 8 Geometric Residual and Rotational Alignment during the treatment session at which the planning CT and CBCT scans were acquired.

	Elapsed Days	Geometric Residual (mm)	Rotation		
			Pitch	Roll	Yaw
Planning CT	0	0.0	0°	0°	0°
CBCT 1	1	1.2	-17.7°	4.8°	-8.1°
CBCT 2	15	1.4	-7.7°	6.9°	-8.1°
CBCT 3	19	1.5	-12.4°	6.5°	-4.9°
CBCT 4	26	1.6	-16.8°	6.9°	-10.6°
CBCT 5	31	1.5	-23.2°	3.7°	-11.3°
CBCT 6	34	1.5	-0.7°	9.4°	-2.5°

The bladder, rectum and prostate volumes are plotted against the elapsed treatment days in Figure 32, below. This figure indicates a dramatic bladder and rectum volume variation over the course of therapy, and this is more significant for the bladder. It also displays a very steady prostate volume over the course of treatment, in contrast to Patient 3. The prostate volume only varies significantly for one treatment session (16% variation), which may have been due to contouring errors because it is difficult to visualize the prostate on the CBCT scans.

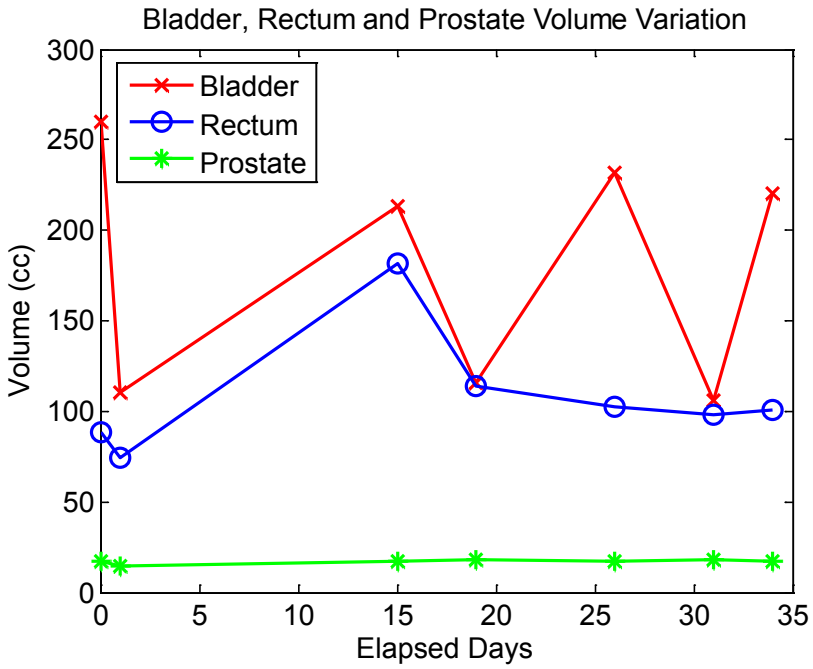

Figure 32: Patient 8 Bladder, Rectum and Prostate volumes measured from the planning CT and CBCT scans and displayed as a function of elapsed days.

The dosimetric indicators for the six CBCT scans and original CT scan were plotted against the daily rotational alignment for Patient 8. The data are presented in terms of the rotational alignment about all three axes separately to determine if there is an obvious trend between rotations about a given axis and the prostate, rectum and bladder dose. The dosimetric indicators for the prostate as the rotational alignment varies in pitch, roll and yaw are displayed in Figure 33, Figure 34 and Figure 35, respectively. The data point referring to a zero degree rotation corresponds to the planning CT scan, where there is no rotational alignment since this scan captures the reference positions of the transponders. The purpose of each of these charts is to display the variation of prostate dose coverage with rotation and the variation of prostate dose

coverage with a decreased planning margin. There appears to be no clear trend in terms of prostate coverage and rotational alignment for rotation in any direction. Better prostate coverage is generally achieved for the 5 mm plans, except for two instances where there is no significant difference between the 5 mm and 3 mm plans. During the treatment session with the largest difference between the 5 mm and 3 mm plans, the percentage of total prostate volume receiving greater than or equal to 100% and 95% of the prescription dose was 99.8% and 100%, respectively, for the 5 mm plan and only 87.5% and 93.0%, respectively, for the 3 mm plan.

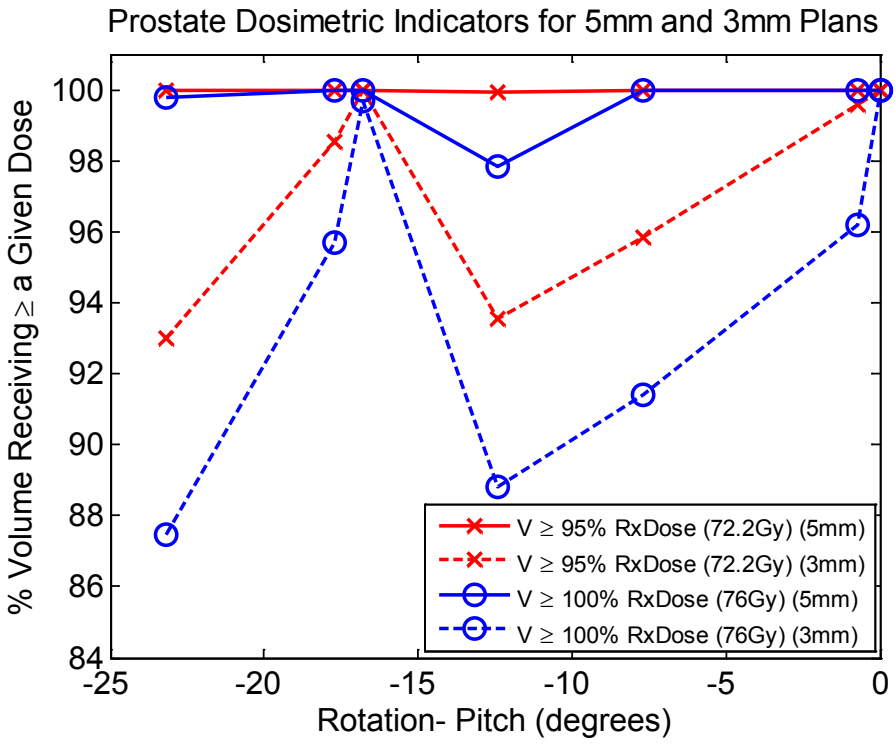

Figure 33: Patient 8 Prostate Dosimetric Indicator variation with rotation (pitch) for 5 mm and 3 mm treatment plans.

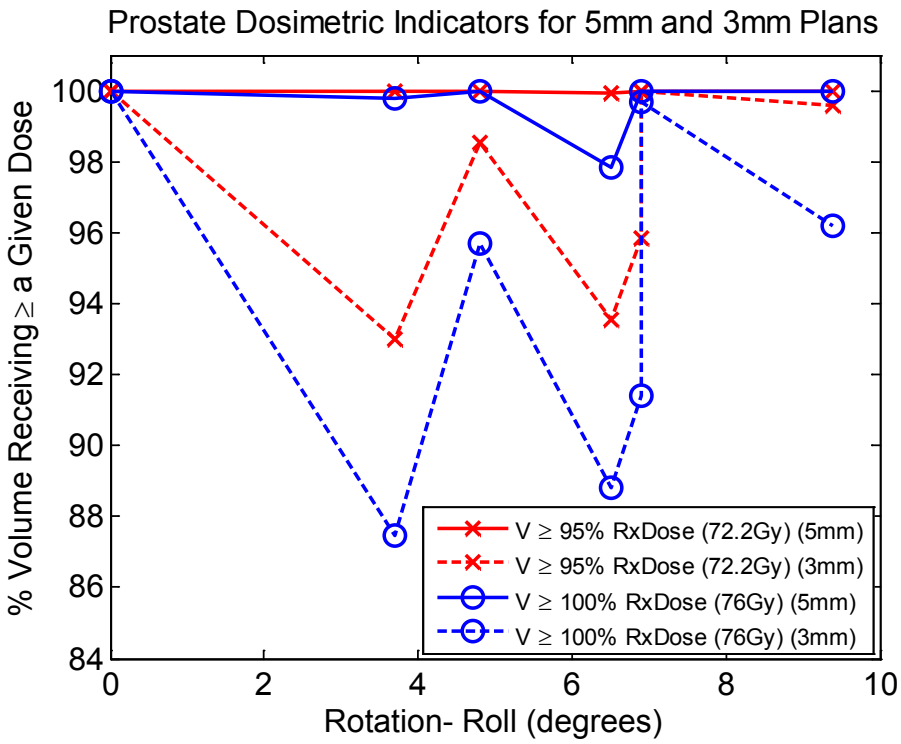

Figure 34: Patient 8 Prostate Dosimetric Indicator variation with rotation (roll) for 5 mm and 3 mm treatment plans.

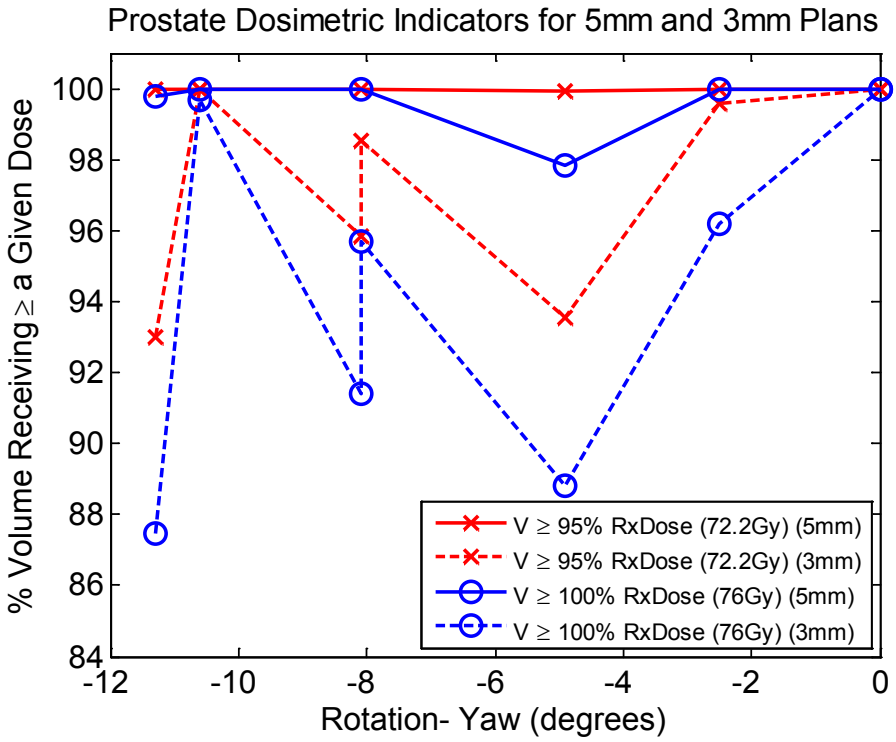

Figure 35: Patient 8 Prostate Dosimetric Indicator variation with rotation (yaw) for 5 mm and 3 mm treatment plans.

The following table (Table 9) displays the minimum dose delivered to the prostate from the 3 mm and 5 mm treatment plans as calculated on the planning CT scan and six CBCT scans. It also displays the elapsed days between a given scan and the first treatment session, the geometric residual and the rotational alignment. This table illustrates the large variation in minimum prostate dose (up to roughly 10.5% between scans with 3 mm plan) that can occur. The minimum prostate dose is much more consistent for the 5 mm plans and only varies by up to 2%. The largest difference in the minimum prostate dose between the 5 mm and 3 mm treatment plans was nearly 10% for the fifth CBCT scan (3 mm plan exhibited the lower minimum prostate dose). Similar

to the results seen in Figure 33, Figure 34 and Figure 35, the minimum prostate doses displayed in Table 9 indicate a significant difference in several cases between the 5 mm and 3 mm treatment plans in terms of prostate coverage for Patient 8.

Table 9: Patient 8 Minimum Dose to the Prostate

	Elapsed Days	Minimum Prostate Dose (Gy) (1cc)		Geometric Residual (mm)	Rotation		
		5 mm Margin	3 mm Margin		Pitch	Roll	Yaw
Planning CT	0	78.5	78.1	0.0	0°	0°	0°
CBCT 1	1	79.2	77.3	1.2	-17.7°	4.8°	-8.1°
CBCT 2	15	78.5	73.9	1.4	-7.7°	6.9°	-8.1°
CBCT 3	19	78.4	71.6	1.5	-12.4°	6.5°	-4.9°
CBCT 4	26	80.0	79.2	1.6	-16.8°	6.9°	-10.6°
CBCT 5	31	78.4	70.9	1.5	-23.2°	3.7°	-11.3°
CBCT 6	34	79.3	76.7	1.5	-0.7°	9.4°	-2.5°

Next, the dosimetric indicators for the rectum as the rotational alignment varies in pitch, roll and yaw are displayed in Figure 36, Figure 37 and Figure 38. No trend between the rotation in any direction and the rectum dose is clear, but large variations in the dosimetric indicators are present. The rectum receives a higher dose from the 5 mm plans as compared to the 3 mm plans and this effect is most significant for the lower dose indicators, similar to the results we saw for the Patient 3. At the lowest dose level (40 Gy), there is a roughly 15 – 20 cc difference between the volume receiving greater than or equal to 40 Gy from the 5 mm and 3 mm plans and this difference decreases to roughly 3 cc for the highest dose level (76 Gy). These rectum dose changes may or may not be clinically significant.

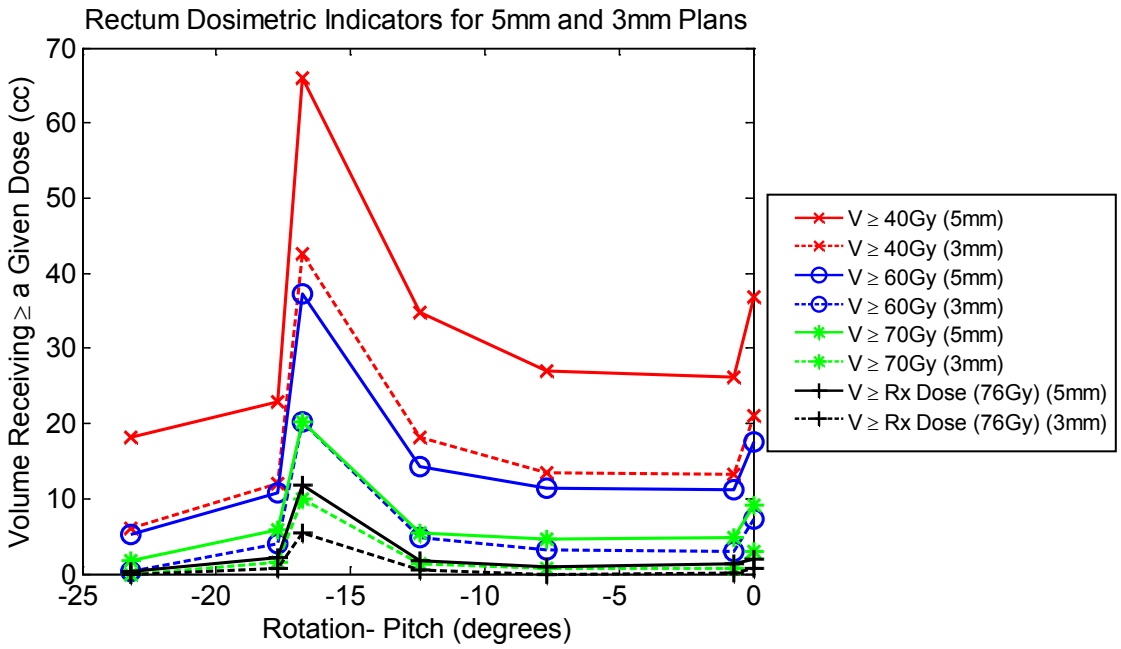

Figure 36: Patient 8 Rectum Dosimetric Indicator Variation with rotation (pitch) for 5 mm and 3 mm treatment plans.

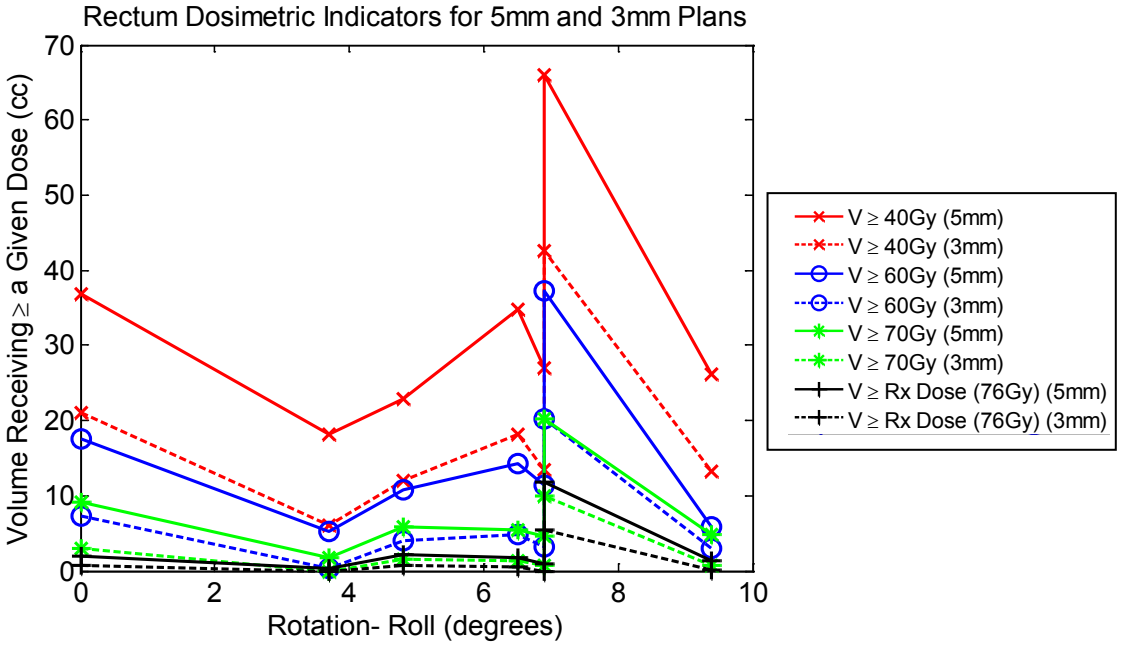

Figure 37: Patient 8 Rectum Dosimetric Indicator Variation with rotation (roll) for 5 mm and 3 mm treatment plans.

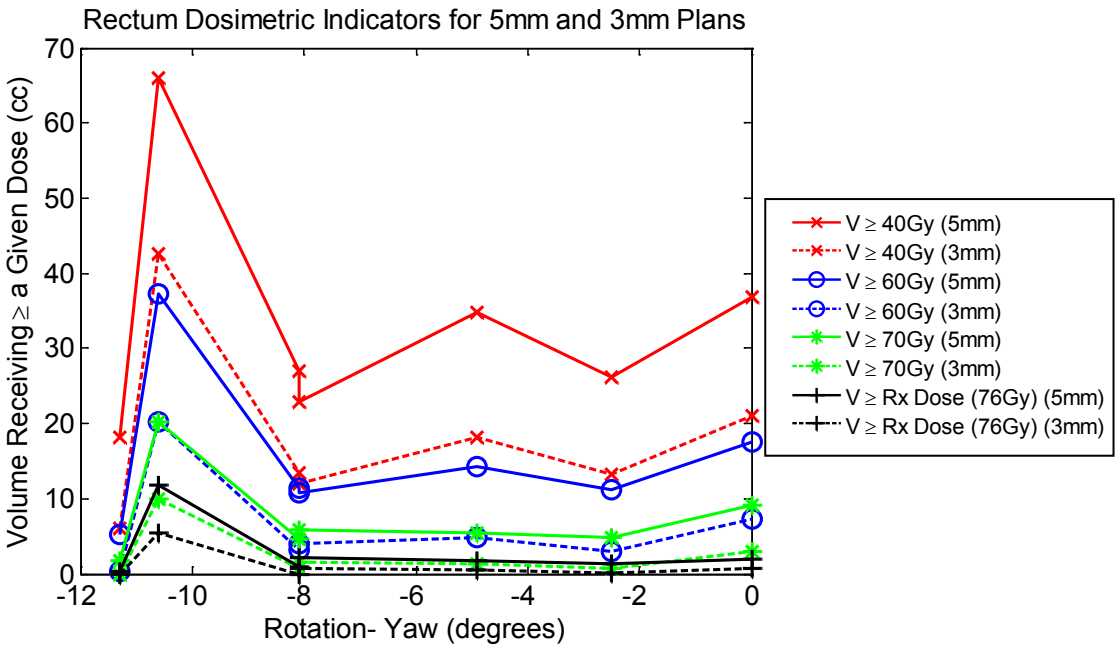

Figure 38: Patient 8 Rectum Dosimetric Indicator Variation with rotation (yaw) for 5 mm and 3 mm treatment plans.

The dosimetric indicators for the bladder as the rotational alignment varies in pitch, roll and yaw are displayed in Figure 39, Figure 40 and Figure 41. As illustrated by these figures, there does not seem to be a strong trend between the bladder dose and the rotation, but similar to the rectum, large variations in the dosimetric indicators are visible. We might have expected the bladder and rectum dose to increase with rotation because the volume changes of these organs, which influence the prostate rotation, may cause the bladder and rectum to expand into the treatment field. The results for both the rectum and bladder suggest that this did not occur. There is an increased dose to the bladder for the 5 mm plans as compared to the 3 mm plans. At the lowest dose level (40 Gy), there is a roughly 20 cc difference between the volume receiving greater than or

equal to 40 Gy from the 5 mm and 3 mm plans and this difference decreases to roughly 6 cc for the highest dose level (76 Gy). As with the change in rectum dose, these relatively small dose changes for the bladder may not be clinically significant.

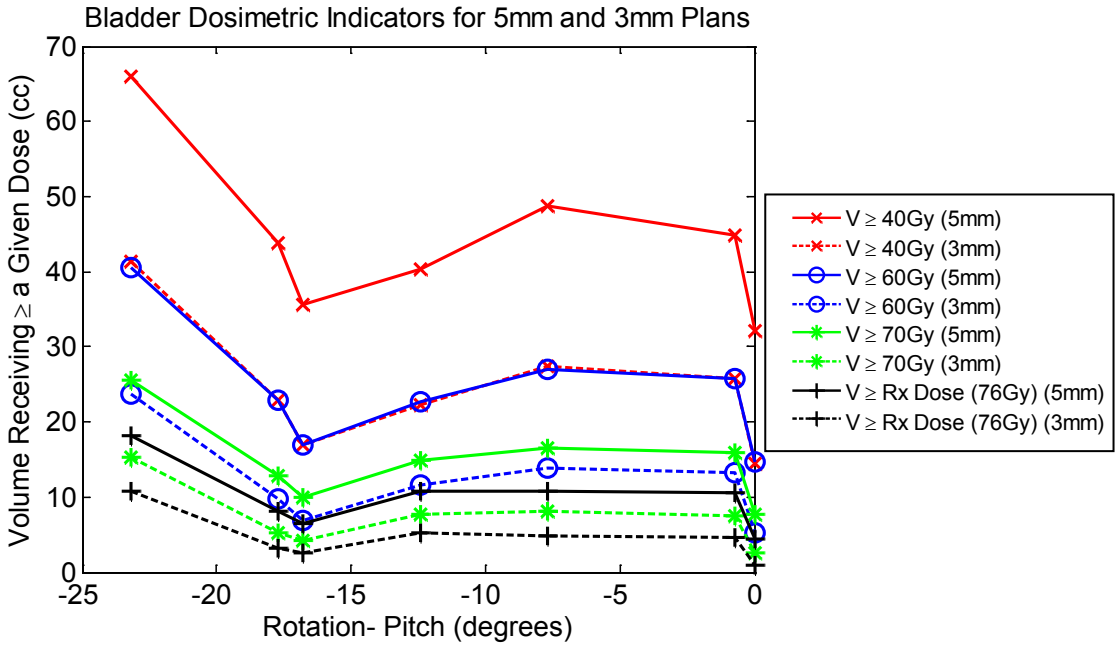

Figure 39: Patient 8 Bladder Dosimetric Indicator Variation with rotation (pitch) for 5 mm and 3 mm treatment plans.

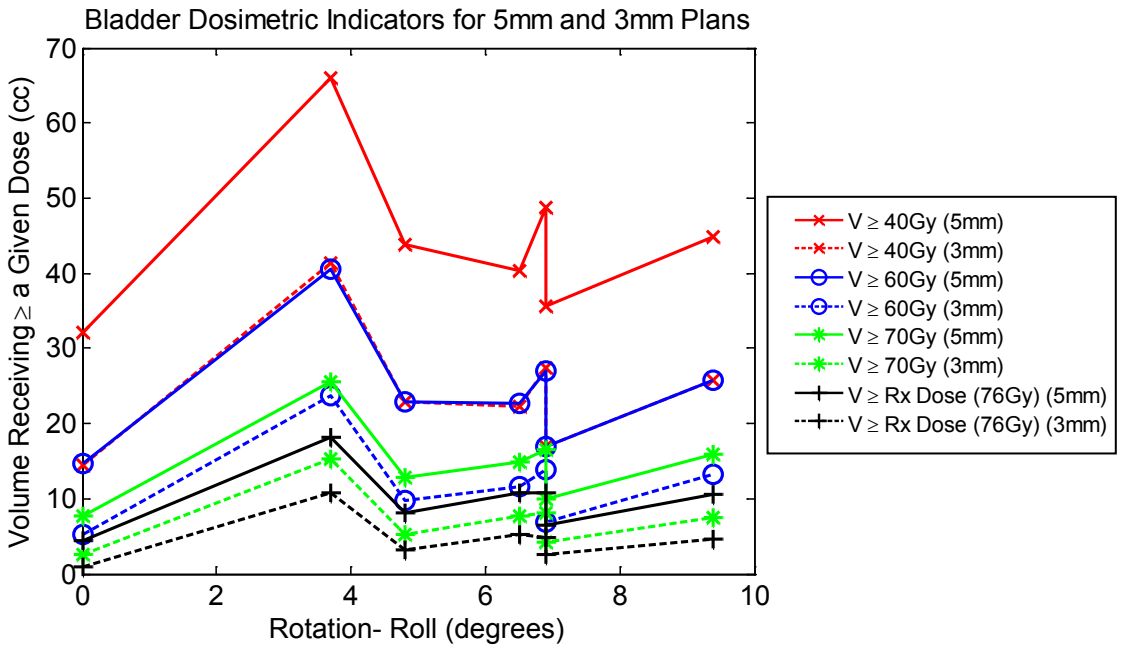

Figure 40: Patient 8 Bladder Dosimetric Indicator Variation with rotation (roll) for 5 mm and 3 mm treatment plans.

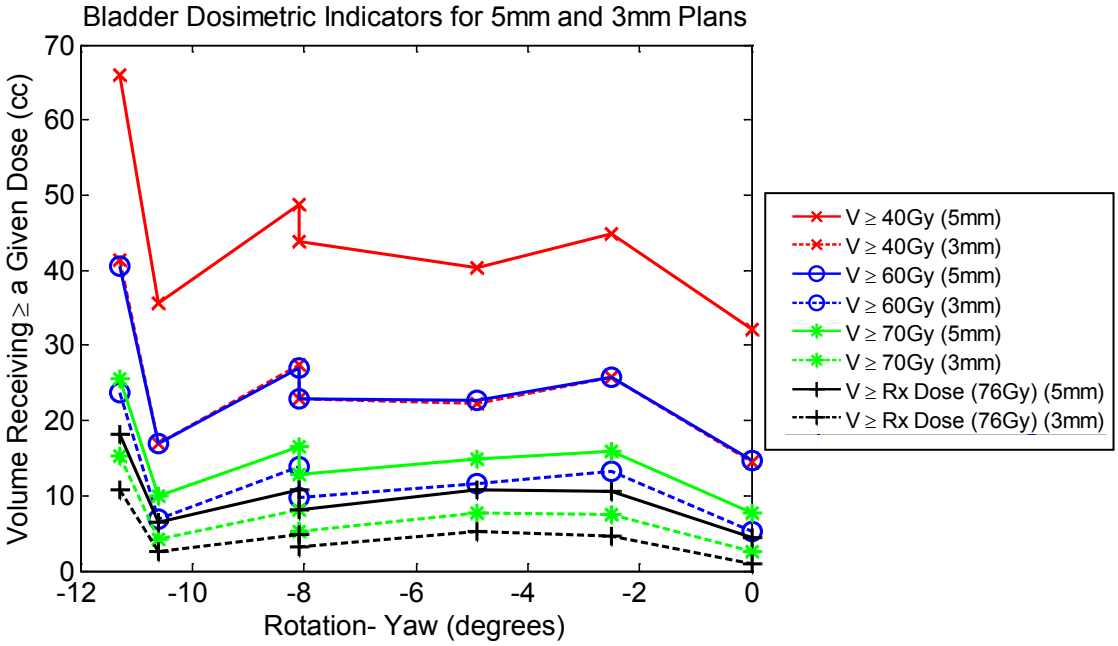

Figure 41: Patient 8 Bladder Dosimetric Indicator Variation with rotation (yaw) for 5 mm and 3 mm treatment plans.

4. Discussion

4.1 Electromagnetic Localization System Accuracy Verification

Previous studies have been performed to verify the submillimeter accuracy of the ELS as compared to planar x-ray imaging (see section 1.1.4.4), however, this work is unique in its use of CBCT imaging as well. Also, the alignments from the ELS and x-ray systems in our study corresponded to the same time point (within ± 1 second) since the ELS tracking continued during image acquisition, whereas several previous studies removed the electromagnetic array just prior to imaging.

The accuracy of the ELS had to be verified prior to eliminating the planar orthogonal imaging because this is the gold standard method of localization for prostate cancer patients with implanted radiopaque markers in the Duke University Department of Radiation Oncology. Subsequent patients treated using the ELS for localization and tracking no longer receive daily planar images but do receive CBCT scans once weekly.

For over half of the patients and the population as a whole, the hypothesized mean difference between the electromagnetic and planar image alignments at which the two populations were indistinguishable was greatest in the AP direction. We have hypothesized that this is because the AP alignment could only be determined from the sagittal image, where the transponders were somewhat obscured by pelvic bony anatomy. A larger hypothesized mean difference was also seen in the AP direction when comparing the electromagnetic and CBCT image alignments. This may have occurred

because the majority of rotations occurred in pitch, affecting the AP displacement more than SI or RL. Our manual best-fit alignment in the AP dimension was different from the ELS's best-fit alignment when using the AP shift to correct for both translation and rotation. Additionally, the precision of the ELS increases slightly with the distance of the transponders from the array and this may have had a small affect on the hypothesized mean difference observed in the AP direction.

4.2 Positional and Rotational Reproducibility of Transponders

We found that the placement of the transponders within the prostate may affect the magnitude of the rotation measured by the ELS. For example, Patient 8 had one transponder located near the prostate-rectum interface due to the random variation in placement by the urologist. For this patient, the transponder located nearest to the prostate-rectum interface represented the long axis of the triangle of the three transponders and we hypothesize that this may have magnified any rotations measured by the ELS. Whether the motion of this transponder represented local prostate deformations or true global rotations is unclear. For those patients whose rotations exceeded the alignment limits, the dosimetry was verified with a CBCT scan, and then the rotational alignment limit was increased as appropriate for that particular patient so that warnings were not triggered during each treatment session.

Two patients, including Patient 3, exhibited a significant decrease in intertransponder distances over the course of treatment. While it is possible that

migration of the transponders caused the intertransponder distance changes, it is more likely that the cause of these changes was prostate shrinkage because all three intertransponder distances decreased steadily and fairly evenly. Additionally, a previous study reported on the significant stability of the transponders throughout a course of treatment[3]. The shrinkage could possibly have been a reaction to radiation treatment, but this is not likely because this trend was not seen for the majority of the other patients. Patient 8 also exhibited an interesting trend in terms of the intertransponder distances. The data for this patient implied that the transponder geometry represented by the planning CT scan was not representative of the day-to-day geometry during treatment. Again, this systematic error may be due to the transponder implant location. We rely on the assumption that the planning CT scan represents the average motion or position of the target but this may not always be true.

4.3 Motion Studies

When analyzing the motion over an entire treatment session, the most motion occurred in the vertical direction because of the large effect and variation of rectal and bladder volume, and the least motion occurred in the lateral direction. Previous studies also noticed the most motion in the vertical and longitudinal directions, primarily from large increases in rectal volume[3,19,24]. From the data presented in Figure 18, Figure 20 and Figure 22, which display the frequency of excursions for the corrected motion data (actual motion), a 5 mm treatment margin to accommodate intrafractional motion

appeared to be adequate. A 3 mm margin for intrafractional motion appeared to be adequate in the lateral direction, however, for the longitudinal and vertical directions, several patients did exhibit motion exceeding 3 mm but it was always less than 10% of the treatment time.

We further analyzed the motion occurring during the first 120 seconds of treatment to simulate an IMAT treatment. We found that using the uncorrected motion data (since these would represent the true data for IMAT patients if the therapists did not perform any repositioning), the excursions greater than 3 mm in the lateral and longitudinal directions and greater than 4 mm in the vertical direction were minimal during the first 120 seconds. This indicates that the probability of needing to interrupt the beam during an IMAT session for our ten patients (using a conventional 5 mm margin) is extremely small. The data displaying the maximum and minimum displacements occurring during the first 120 seconds of each patient's treatment for Patients 1 and 3 indicate that the displacements were within 5 mm and thus a 5 mm margin should be adequate during an IMAT treatment when repositioning was not performed. These data also indicate that the target excursions increase in frequency and magnitude with time.

4.4 Margin Analysis

Margin analysis was also performed quantitatively using a margin formula by van Herk, et al[1]. The margins generated were fairly small compared with the 5 mm

margin currently used for patients being localized and continuously tracked using the ELS. Several factors may have contributed to the small margins generated with the formula. First, the formula does not account for rotations or shape variations (deformations) of the target. Second, the formula assumes the use of 3D conformal radiation therapy rather than IMRT. The use of IMRT results in steeper dose gradients. Thus, a target displacement may have a greater dosimetric impact during IMRT than during 3D conformal radiation therapy and a larger margin may be necessary.

It is also interesting to note that the margins generated for the population are much smaller than those generated for the individual patients. This likely resulted from the constraints utilized by the formula, which required that the minimum dose to the CTV be 95% of the prescription dose or higher for 90% of the population. While this may not be the ideal situation (ideal situation would require the minimum dose to the CTV to be 100% of the prescription dose for 100% of the population), it is adequate for this study. The non-ideal constraints allowed coverage to be compromised for the most often and largely displaced patients in the population analysis, resulting in smaller margins than were determined for nearly all individual patients. Since a 3 mm margin was found to be suitable using this margin formula for the majority of patients using the corrected (actual) motion data, this was the margin used during the dosimetric analysis to test the possible benefit of a decreased planning margin. Melancon, et al., also found that a 3

mm planning margin was adequate to account for intrafractional motion for most patients[19].

4.5 Dosimetric Analysis

Dosimetric analysis was performed for two patients (Patients 3 and 8) who exhibited some of the largest variations in geometric residual, intertransponder distances and rotational alignment over the course of radiation therapy. We investigated the impact of the prostate deformations on the prostate dose coverage, as well as the bladder and rectal doses. The seminal vesicles were ignored in this analysis but the variation in coverage of this structure should be considered in the future. Given that the seminal vesicles are smaller and exhibit more motion and deformation than the prostate, the variation in coverage for the seminal vesicles may be more dramatic than for the prostate[18]. We also investigated whether a decreased planning margin (3 mm) would be adequate for these two patients, given the hypothesized prostate shrinkage for Patient 3 and the large prostate rotations measured for Patient 8.

Using the volumes determined from the contours on the planning CT and subsequent CBCT scans for Patient 3, we found that the prostate volume decreased by roughly 20% between the planning CT scan and the last CBCT scan, but it is possible that this was due to variation in contouring on the CBCT scans since it is very difficult to visualize the prostate. If prostate shrinkage did indeed occur, we might have expected the rectum and bladder dose to increase with prostate shrinkage and increasing

geometric residual because this may cause more of the bladder and rectum to be located in the treatment field. Interestingly, though, we saw variable bladder and rectum doses but did not discern any noticeable trend in terms of dose and geometric residual.

When considering a smaller planning margin for Patient 3, we found that the prostate coverage for the 3 mm plan was comparable to the 5 mm plan and the dose to the rectum and bladder was decreased. This indicated that a 3 mm margin may be beneficial in terms of bladder and rectal sparing while still maintaining adequate coverage of the prostate. It still remains to be investigated whether the decreases in bladder and rectum doses will produce clinically observable results.

No clear trends in terms of prostate, rectum and bladder dose and rotation were visible for Patient 8, though the doses were quite variable. Because rectum and bladder filling influence the rotation of the prostate, we might have expected the dose to these organs to increase with rotation if they were also expanding into the treatment field, but this effect was not seen. Additionally, our sample sizes may not be large enough to show correlation of dose with either rotation or geometric residual for Patients 8 and 3, respectively. We also did not notice any clear correlation between rectum and bladder volumes and prostate coverage, similar to a previous study[19].

When considering a smaller planning margin for Patient 8, we found that the prostate coverage for the 3 mm plan was worse in comparison to the 5 mm plan in several cases. Even with the decreased dose to the rectum and bladder for the 3 mm

plan, a smaller margin would not be recommended for Patient 8 given that our primary concern is the prostate and it received inadequate coverage. As mentioned above, the clinical significance of the observable dose differences to the rectum and bladder needs to be determined. It is important to note that the 5 mm plan which was actually used to treat Patient 8 provided sufficient prostate coverage.

Given the variable results between Patients 3 and 8 in terms of a decreased planning margin, it would be difficult to formulate a single margin recommendation for future ELS patients. Several options are available. First, the use of a 5 mm margin for all patients could continue to be used. Alternatively, both a 5 mm and 3 mm plan could be created for each patient based on the planning CT scan, and CBCT scans could be obtained during the first five fractions. By calculating the potential dose from both plans on the CBCT scans and evaluating the two dose distributions, a recommendation for which plan to use for the subsequent treatments could be made. A third solution would be to treat each patient using the standard 5 mm margin for the first five treatment sessions and then use the motion and rotation information acquired during the first week of treatment to design an individualized treatment margin that would be used during the subsequent treatment sessions. These solutions introduce multiple complicating factors including additional time devoted to creating two plans and performing two IMRT QAs, but they highlight the issues that must be considered when implementing a new procedure for determining suitable planning margins. Prior to

implementing the last two solutions presented above, an investigation into the true benefit of utilizing a decreased planning margin in terms of critical organ sparing must be performed.

5. Conclusions

Electromagnetic alignments are accurate to within 1 mm as compared to planar and CBCT x-ray alignments. Changes in transponder geometry over the course of therapy seem to be related to prostate volume reduction and transponder implant location. All patients fell within the default geometric residual (2mm), and most within the default rotational alignment (10°) limits, though several patients exceeded this default limit on multiple occasions and a CBCT scan was acquired to verify the dosimetry when this occurred.

The majority of excursions occurring during an entire treatment session (when uncorrected motion data were used) were less than 5 mm in all directions and the largest and most frequent excursions occurred in the AP direction. The frequency of excursions decreased when the patient repositioning was accounted for (when corrected motion data were used). The frequency of excursions was even less when considering only the first 120 seconds of a treatment session, to simulate an IMAT treatment. The excursions occurring during the first 120 seconds of treatment were less than 4 mm (> 99% of measurements), indicating that a 5 mm margin, as used for conventional IMRT treatments, should be adequate to account for intrafractional motion. With this margin, the likelihood of having to interrupt the radiation delivery to reposition the patient during an IMAT treatment would be very small.

Margin analysis using a formula developed by van Herk, et al., generated margins that were less than 3 mm for the majority of patients when corrected motion data were used[1]. From the dosimetric analysis, a 3 mm margin appeared to be adequate for the patient with the largest measured translational transponder displacement (Patient 3), but did not provide the necessary prostate coverage for the patient with the largest rotational transponder displacement (Patient 8). The plans using a 5 mm margin, which were actually delivered during treatment, provided sufficient prostate coverage for both patients. Multiple factors must be considered prior to implementing a smaller planning margin and the margin may need to be determined on a patient-specific basis.

Appendix A: Tabulated Motion Data

The frequency of excursions > 1 mm, > 2 mm, > 3 mm, > 4 mm and > 5 mm occurring during a treatment session was determined for each patient using corrected and uncorrected motion data. These data are presented for each patient in the lateral, longitudinal and vertical directions. The frequency of the uncorrected lateral, longitudinal and vertical target excursions is displayed in Table 10, Table 11 and Table 12, respectively. The frequency of the corrected lateral, longitudinal and vertical target excursions is displayed in Table 13, Table 14 and Table 15, respectively. The frequency of excursions occurring during the first 120 seconds of a treatment session was also determined for each patient using the uncorrected motion data. These data are presented below in Table 16, Table 17 and Table 18.

Table 10: Frequency of lateral uncorrected target excursions during the entire treatment session.

	Magnitude of Lateral (x) Excursion				
Patient	x > 1 mm	x > 2 mm	x > 3 mm	x > 4 mm	x > 5 mm
1	18.49%	0.00%	0.00%	0.00%	0.00%
2	8.36%	0.88%	0.00%	0.00%	0.00%
3	18.53%	2.41%	0.00%	0.00%	0.00%
4	13.44%	2.01%	0.00%	0.00%	0.00%
5	40.00%	9.26%	2.16%	0.14%	0.00%
6	43.66%	14.73%	1.03%	0.01%	0.00%
7	21.75%	2.33%	0.00%	0.00%	0.00%
8	21.52%	2.65%	0.00%	0.00%	0.00%
9	15.33%	2.68%	0.00%	0.00%	0.00%
10	41.65%	9.61%	2.39%	0.01%	0.00%

Table 11: Frequency of longitudinal uncorrected target excursions during the entire treatment session.

	Magnitude of Longitudinal (y) Excursion				
Patient	y > 1 mm	y > 2 mm	y > 3 mm	y > 4 mm	y > 5 mm
1	26.73%	4.13%	0.04%	0.00%	0.00%
2	25.28%	2.33%	0.00%	0.00%	0.00%
3	54.71%	20.57%	3.20%	0.49%	0.00%
4	39.49%	3.53%	0.20%	0.01%	0.00%
5	43.87%	8.57%	1.57%	0.06%	0.00%
6	50.55%	22.28%	6.66%	2.68%	1.86%
7	31.95%	6.78%	1.91%	0.01%	0.00%
8	52.67%	17.59%	2.63%	0.61%	0.02%
9	17.67%	4.72%	0.03%	0.00%	0.00%
10	28.08%	8.68%	2.80%	0.77%	0.00%

Table 12: Frequency of vertical uncorrected target excursions during the entire treatment session.

	Magnitude of Vertical (z) Excursion				
Patient	z > 1 mm	z > 2 mm	z > 3 mm	z > 4 mm	z > 5 mm
1	43.29%	5.93%	0.00%	0.00%	0.00%
2	59.36%	21.50%	3.95%	0.39%	0.00%
3	65.91%	36.52%	13.79%	2.84%	0.24%
4	42.42%	11.70%	2.23%	1.00%	0.30%
5	52.32%	10.63%	1.48%	0.01%	0.00%
6	65.38%	37.39%	17.06%	4.99%	1.48%
7	57.31%	10.07%	0.36%	0.00%	0.00%
8	51.10%	11.66%	0.73%	0.05%	0.00%
9	54.72%	13.31%	0.56%	0.00%	0.00%
10	68.23%	36.82%	17.23%	9.76%	3.40%

Table 13: Frequency of lateral corrected target excursions during the entire treatment session.

	Magnitude of Lateral (x) Excursion				
Patient	x > 1 mm	x > 2 mm	x > 3 mm	x > 4 mm	x > 5 mm
1	18.49%	0.00%	0.00%	0.00%	0.00%
2	8.36%	0.88%	0.00%	0.00%	0.00%
3	16.34%	1.02%	0.00%	0.00%	0.00%
4	13.43%	2.01%	0.00%	0.00%	0.00%
5	37.54%	7.87%	0.79%	0.00%	0.00%
6	35.71%	7.87%	0.02%	0.00%	0.00%
7	20.98%	2.33%	0.00%	0.00%	0.00%
8	19.58%	0.99%	0.00%	0.00%	0.00%
9	15.33%	2.68%	0.00%	0.00%	0.00%
10	32.78%	5.88%	0.42%	0.00%	0.00%

Table 14: Frequency of longitudinal corrected target excursions during the entire treatment session.

	Magnitude of Longitudinal (y) Excursion				
Patient	y > 1 mm	y > 2 mm	y > 3 mm	y > 4 mm	y > 5 mm
1	26.73%	4.13%	0.04%	0.00%	0.00%
2	25.28%	2.33%	0.00%	0.00%	0.00%
3	50.26%	17.34%	1.93%	0.04%	0.00%
4	39.44%	3.53%	0.20%	0.01%	0.00%
5	40.90%	7.00%	0.92%	0.00%	0.00%
6	48.56%	19.37%	5.62%	2.25%	1.27%
7	31.93%	6.77%	1.69%	0.00%	0.00%
8	50.58%	17.17%	2.28%	0.61%	0.02%
9	17.67%	4.72%	0.03%	0.00%	0.00%
10	25.00%	3.99%	0.37%	0.00%	0.00%

Table 15: Frequency of vertical corrected target excursions during the entire treatment session.

	Magnitude of Vertical (z) Excursion				
Patient	z > 1 mm	z > 2 mm	z > 3 mm	z > 4 mm	z > 5 mm
1	42.38%	5.90%	0.00%	0.00%	0.00%
2	59.36%	21.50%	3.95%	0.39%	0.00%
3	59.24%	29.05%	6.78%	0.13%	0.06%
4	41.52%	10.15%	1.16%	0.41%	0.13%
5	49.43%	8.39%	0.07%	0.00%	0.00%
6	56.04%	26.47%	9.99%	1.55%	0.15%
7	56.84%	9.75%	0.36%	0.00%	0.00%
8	50.65%	11.48%	0.73%	0.04%	0.00%
9	54.72%	13.31%	0.56%	0.00%	0.00%
10	61.85%	24.95%	5.50%	0.44%	0.13%

Table 16: Frequency of lateral uncorrected target excursions during the first 120 seconds of the treatment session.

	Magnitude of Lateral (x) Excursion				
Patient	x > 1 mm	x > 2 mm	x > 3 mm	x > 4 mm	x > 5 mm
1	16.43%	0.00%	0.00%	0.00%	0.00%
2	6.77%	0.02%	0.00%	0.00%	0.00%
3	12.48%	2.03%	0.00%	0.00%	0.00%
4	15.56%	2.63%	0.00%	0.00%	0.00%
5	24.86%	5.39%	0.00%	0.00%	0.00%
6	43.74%	8.87%	0.00%	0.00%	0.00%
7	22.88%	1.65%	0.00%	0.00%	0.00%
8	17.01%	1.17%	0.00%	0.00%	0.00%
9	14.03%	2.71%	0.00%	0.00%	0.00%
10	35.53%	6.85%	0.58%	0.00%	0.00%

Table 17: Frequency of longitudinal uncorrected target excursions during the first 120 seconds of the treatment session.

	Magnitude of Longitudinal (y) Excursion				
Patient	y > 1 mm	y > 2 mm	y > 3 mm	y > 4 mm	y > 5 mm
1	20.95%	1.46%	0.00%	0.00%	0.00%
2	21.42%	0.33%	0.00%	0.00%	0.00%
3	43.33%	11.45%	1.15%	0.00%	0.00%
4	39.31%	2.54%	0.06%	0.00%	0.00%
5	36.57%	2.60%	0.00%	0.00%	0.00%
6	42.19%	10.13%	0.93%	0.00%	0.00%
7	28.15%	4.40%	0.88%	0.00%	0.00%
8	43.67%	13.07%	0.42%	0.18%	0.00%
9	15.04%	4.56%	0.00%	0.00%	0.00%
10	22.24%	5.58%	0.32%	0.00%	0.00%

Table 18: Frequency of vertical uncorrected target excursions during the first 120 seconds of the treatment session.

	Magnitude of Vertical (z) Excursion				
Patient	z > 1 mm	z > 2 mm	z > 3 mm	z > 4 mm	z > 5 mm
1	38.67%	2.87%	0.00%	0.00%	0.00%
2	45.68%	15.22%	0.64%	0.00%	0.00%
3	55.27%	23.94%	6.84%	0.49%	0.00%
4	39.77%	7.94%	0.53%	0.11%	0.00%
5	56.81%	4.58%	0.10%	0.00%	0.00%
6	60.87%	31.86%	8.23%	0.00%	0.00%
7	53.67%	4.65%	0.21%	0.00%	0.00%
8	50.06%	12.18%	0.10%	0.00%	0.00%
9	41.08%	8.05%	0.00%	0.00%	0.00%
10	49.65%	19.65%	4.51%	0.74%	0.02%

References

1. van Herk, M., Remeijer, P., Rasch, C., & Lebesque, J. V. (2000). The Probability of Correct Target Dosage: Dose-Population Histograms for Deriving Treatment Margins in Radiotherapy. *International Journal of Radiation Oncology Biology Physics, 47* (4), 1121-1135.

2. Willoughby, T. R., Kupelian, P. A., Pouliot, J., Shinohara, K., Aubin, M., Roach, I. M., et al. (2006). Target Localization and Real-Time Tracking Using the Calypso 4D Localization System in Patients with Localized Prostate Cancer. *International Journal of Radiation Oncology Biology Physics, 65* (2), 528-534.

3. Kupelian, P., Willoughby, T., Mahadevan, A., Djemil, T., Weinstein, G., Jani, S., et al. (2007). Multi-Institutional Clinical Experience With the Calypso System in Localization and Continuous, Real-Time Monitoring of the Prostate Gland During External Radiotherapy. *International Journal of Radiation Oncology Biology Physics, 67* (4), 1088-1098.

4. Litzenberg, D., Dawson, L. A., Sandler, H., Sanda, M. G., McShan, D. L., Ten Haken, R. K., et al. (2002). Daily Prostate Targeting Using Implanted Radiopaque Markers. *International Journal of Radiation Oncology Biology Physics, 52* (3), 699-703.

5. Langen, K. M., Willoughby, T. R., Meeks, S. L., Santhanam, A., Cunningham, A., Levine, L., et al. (2008). Observations on Real-Time Prostate Gland Motion Using Electromagnetic Tracking. *International Journal of Radiation Oncology Biology Physics, 71* (4), 1084-1090.

6. Nederveen, A. J., Dehnad, H., van der Heide, U. A., van Moorselaar, R. J., Hofman, P., & Lagendijk, J. J. (2003). Comparison of Megavoltage Position Verification for Prostate Irradiation Based on Bony Anatomy and Implanted Fiducials. *Radiotherapy and Oncology, 68*, 81-88.

7. Bortfeld, T., Jiang, S. B., & Rietzel, E. (2004). Effects of Motion on the Total Dose Distribution. *Seminars in Radiation Oncology, 14* (1), 41-51.

8. Storey, M. R., Pollack, A., Zagars, G., Smith, L., Antolak, J., & Rosen, I. (2000). Complications from Radiotherapy Dose Escalation in Prostate Cancer: Preliminary Results of a Randomized Trial. *International Journal of Radiation Oncology Biology Physics, 48* (3), 635-642.

9. Vargas, C., Martinez, A., Kestin, L. L., Yan, D., Grills, I., Brabbins, D. S., et al. (2005). Dose-Volume Analysis of Predictors for Chronic Rectal Toxicity After Treatment of Prostate Cancer with Adaptive Image-Guided Radiotherapy. *International Journal of Radiation Oncology Biology Physics, 62* (5), 1297-1308.

10. O'Daniel, J. C., Dong, L., Zhang, L., de Crevoisier, R., Wang, H., Lee, A. K., et al. (2006). Dosimetric Comparison of Four Target Alignment Methods for Prostate Cancer Radiotherapy. *International Journal of Radiation Oncology Biology Physics, 66* (3), 883-891.

11. Balter, J. M., Sandler, H. M., Lam, K., Bree, R. L., Lichter, A. S., & Ten Haken, R. K. (1995). Measurement of Prostate Movement over the Course of Routine Radiotherapy Using Implanted Markers. *International Journal of Radiation Oncology Biology Physics, 31* (1), 113-118.

12. Wong, J. R., Grimm, L., Uematsu, M., Oren, R., Cheng, C. W., Merrick, S., et al. (2005). Image-Guided Radiotherapy for Prostate Cancer by CT-Linear Accelerator Combination: Prostate Movements and Dosimetric Considerations. *International Journal of Radiation Oncology Biology Physics, 61* (2), 561-569.

13. Noel, C., Parikh, P., Roy, M., Kupelian, P., Mahadevan, A., Weinstein, G., et al. (2008). Prediction of Intrafraction Prostate Motion: Accuracy of Pre- and Post-Treatment Imaging and Intermittent Imaging. *International Journal of Radiation Oncology Biology Physics*, 1-7.

14. *Patient Resources: Prostate Radiation Therapy and Organ Motion*. Retrieved 2009, from Calypso Medical web site: http://www.calypsomedical.com.

15. Zhu, X., Bourland, J. D., Yuan, Y., Zhuang, T., O'Daniel, J., Thongphiew, D., et al. (2009). Tradeoffs of Integrating Real-Time Tracking into IGRT for Prostate Cancer Treatment. *Physics in Medicine and Biology, 54*, 393-401.

16. Calypso Medical Technologies, Inc. Calypso 4D Localization System User's Manual. 2007. Seattle, WA.

17. Balter, J. M., Wright, J. N., Newell, L. J., Friemel, B., Dimmer, S., Cheng, Y., et al. (2005). Accuracy of a Wireless Localization System for Radiotherapy. *International Journal of Radiation Oncology Biology Physics, 61* (3), 933-937.

18. Santanam, L., Malinowski, K., Hubenshmidt, J., Dimmer, S., Mayse, M. L., Bradley, J., et al. (2008). Fiducial-Based Translational Localization Accuracy of

Electromagnetic Tracking System and On-Board Kilovoltage Imaging System. *International Journal of Radiation Oncology Biology Physics, 70* (3), 892-899.

19. Melancon, A. D., O'Daniel, J. C., Zhang, L., Kudchadker, R. J., Kuban, D. A., Lee, A. K., et al. (2007). Is a 3-mm Intrafractional Margin Sufficient for Daily Image-Guided Intensity-Modulated Radiation Therapy of Prostate Cancer? *Radiotherapy and Oncology, 85*, 251-259.

20. Purdy, J. A. (2004). Current ICRU Definitions of Volumes: Limitations and Future Directions. *Seminars in Radiation Oncology, 14* (1), 27-40.

21. Kahn, F. M. (2003). *The Physics of Radiation Therapy* (3rd Edition ed.). Philadelphia, PA, USA: Lippincott Williams & Wilkins .

22. Santanam, L., Noel, C., Willoughby, T. R., Esthappan, J., Mutic, S., Klein, E. E., et al. (2009). Quality Assurance for Clinical Implementation of an Electromagnetic Tracking System. *Medical Physics, 36* (8), 3477-3486.

23. van Herk, M. (2004). Errors and Margins in Radiotherapy. *Seminars in Radiation Oncology, 14* (1), 52-64.

24. Nederveen, A. J., van der Heide, U. A., Dehnad, H., van Moorselaar, R. J., Hofman, P., & Lagendijk, J. J. (2002). Measurements and Clinical Consequences of Prostate Motion During a Radiotherapy Fraction. *International Journal of Radiation Oncology Biology Physics, 53* (1), 206-214.

25. Hoogeman, M. S., van Herk, M., de Bois, J., & Lebesque, J. V. (2005). Strategies to Reduce the Systematic Error Due to Tumor and Rectum Motion in Radiotherapy of Prostate Cancer. *Radiotherapy and Oncology, 74*, 177-185.

26. Quigley, M. M., Mate, T. P., & Sylvester, J. E. (2009). Prostate Tumor Alignment and Continuous, Real-Time Adaptive Radiation Therapy Using Electromagnetic Fiducials: Clinical and Cost-Utility Analyses. *Urologic Oncology: Seminars and Original Investigations, 27*, 473-482.

27. Yan, D., Vicini, F., Wong, J., & Martinez, A. (1997). Adaptive Radiation Therapy. *Physics in Medicine and Biology, 42*, 123-132.

28. Yoo, S., & Yin, F.-F. (2006). Dosimetric Feasibility of Cone-Beam CT-Based Treatment Planning Compared to CT-Based Treatment Planning. *International Journal of Radiation Oncology Biology Physics, 66* (5), 1553-1561.